

Topological conformal defects with tensor networks

Markus Hauru,^{1,2,*} Glen Evenbly,³ Wen Wei Ho,⁴ Davide Gaiotto,¹ and Guifre Vidal¹

¹*Perimeter Institute for Theoretical Physics, Waterloo, Ontario N2L 2Y5, Canada*

²*Department of Physics and Astronomy, University of Waterloo, Waterloo, Ontario, Canada, N2L 3G1.*

³*Department of Physics and Astronomy, University of California, Irvine, CA 92697-4575 USA*

⁴*Department of Theoretical Physics, University of Geneva,
24 quai Ernest-Ansermet, 1211 Geneva, Switzerland*

(Dated: February 2, 2022)

The critical two-dimensional classical Ising model on the square lattice has two topological conformal defects: the \mathbb{Z}_2 symmetry defect D_ϵ and the Kramers-Wannier duality defect D_σ . These two defects implement antiperiodic boundary conditions and a more exotic form of twisted boundary conditions, respectively. On the torus, the partition function Z_D of the critical Ising model in the presence of a topological conformal defect D is expressed in terms of the scaling dimensions Δ_α and conformal spins s_α of a distinct set of primary fields (and their descendants, or conformal towers) of the Ising conformal field theory. This characteristic conformal data $\{\Delta_\alpha, s_\alpha\}_D$ can be extracted from the eigenvalue spectrum of a transfer matrix M_D for the partition function Z_D . In this paper, we investigate the use of tensor network techniques to both represent and coarse-grain the partition functions Z_{D_ϵ} and Z_{D_σ} of the critical Ising model with either a symmetry defect D_ϵ or a duality defect D_σ . We also explain how to coarse-grain the corresponding transfer matrices M_{D_ϵ} and M_{D_σ} , from which we can extract accurate numerical estimates of $\{\Delta_\alpha, s_\alpha\}_{D_\epsilon}$ and $\{\Delta_\alpha, s_\alpha\}_{D_\sigma}$. Two key new ingredients of our approach are (i) coarse-graining of the defect D , which applies to any (i.e. not just topological) conformal defect and yields a set of associated scaling dimensions Δ_α , and (ii) construction and coarse-graining of a generalized translation operator using a local unitary transformation that moves the defect, which only exist for topological conformal defects and yields the corresponding conformal spins s_α .

I. INTRODUCTION

A conformal defect is a universality class of critical behavior at the junction of two critical systems. Relevant examples include point impurities, interfaces and boundary phenomena in critical 1D quantum systems, as well as line defects, interfaces and boundaries in critical 2D classical systems^{1–5}. A *topological* conformal defect in a conformal field theory (CFT) is a particular type of conformal defect that is totally transmissive⁵ and can be deformed without affecting the value of correlators as long as it is not taken across a field insertion. It can also be regarded as defining a form of twisted boundary conditions for that CFT.

The goal of this paper is to investigate the use of tensor network techniques to describe topological conformal defects in microscopic lattice models. For simplicity, we analyze the two-dimensional critical Ising model, working mostly with the 2D classical statistical spin system, but also repeatedly connecting to the (1+1)D quantum spin chain. The critical Ising model turns out to have two non-trivial topological conformal defects: a symmetry defect D_ϵ and a duality defect D_σ ⁶. The symmetry defect D_ϵ relates to the global \mathbb{Z}_2 spin-flip symmetry of the Ising model and implements antiperiodic boundary conditions, whereas the duality defect D_σ relates to the Kramers-Wannier self-duality of the critical Ising model and can be thought of as implementing some form of twisted boundary conditions.

A. Defects and transfer matrices

Consider the statistical partition function Z of the critical 2D classical Ising model on a square lattice with periodic boundary conditions (that is, on a torus), made of $m \times n$ sites. By the operator-state correspondence of CFT², this partition function is expressed in terms of the scaling dimensions Δ_α and conformal spins s_α of some specific set of scaling operators ϕ_α , namely, those in the conformal towers of the three local primary fields of the Ising CFT: the identity, energy-density and spin primaries. We can extract $\{\Delta_\alpha, s_\alpha\}$ from the spectrum of eigenvalues of a transfer matrix M for the partition function Z , fulfilling $Z = \text{Tr}(M^m)$ [see Fig. 1(a)].

In the presence of a topological conformal defect D , the modified partition function Z_D is expressed now in terms of the scaling dimensions and conformal spins $\{\Delta_\alpha, s_\alpha\}_D$ of other conformal towers, corresponding to a different set of primary fields. We can again extract $\{\Delta_\alpha, s_\alpha\}_D$ from the spectrum of eigenvalues of a modified transfer matrix M_D for the partition function Z_D , fulfilling $Z_D = \text{Tr}((M_D)^m)$ [see Fig. 1(b)].

In this paper, we build tensor network representations of the transfer matrices M_{D_ϵ} and M_{D_σ} for the two topological conformal defects D_ϵ and D_σ of the critical Ising model and explain how to extract accurate estimates of the corresponding scaling dimensions and conformal spins $\{\Delta_\alpha, s_\alpha\}_{D_\epsilon}$ and $\{\Delta_\alpha, s_\alpha\}_{D_\sigma}$, which we regard as a characterization of these defects. These estimates are obtained by first coarse-graining and then diagonalizing the transfer matrices M_{D_ϵ} and M_{D_σ} .

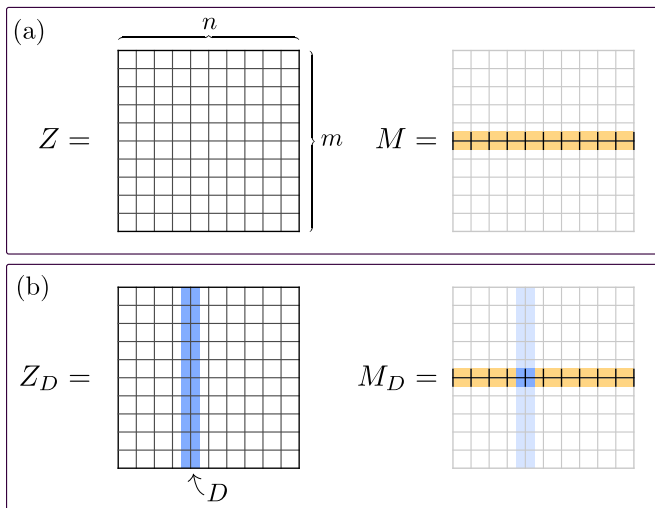


Figure 1. (a) Partition function Z on a square lattice made of $n \times m$ sites with periodic boundary conditions in both directions (a torus), and the corresponding transfer matrix M , such that $Z = \text{Tr}(M^m)$. (b) Partition function Z_D on the same torus, where the defect D implements some form of boundary conditions, and the generalized transfer matrix M_D , such that $Z_D = \text{Tr}((Z_D)^m)$.

We emphasize that on a sufficiently small $m \times n$ torus, say in the range $n \sim 10 - 20$, one can already diagonalize the transfer matrix M_D for defect D , and thus obtain numerical estimates of $\{\Delta_\alpha, s_\alpha\}_D$, by using exact diagonalization techniques. Why do we then need to use tensor networks? As we will review, these estimates for $\{\Delta_\alpha, s_\alpha\}_D$ are affected by non-universal, finite-size corrections, which diminish with growing n . The merit of tensor network techniques is then merely that, through proper coarse-graining, they allow us to consider a much larger n than exact diagonalization techniques, thus producing more accurate numerical estimates. However, the coarse-graining of the tensor network introduces *truncation errors*, which must be kept under check and effectively limit the size n that can be reliably considered.

In the absence of defects, the use of tensor networks to obtain more accurate estimates of the conformal data $\{\Delta_\alpha, s_\alpha\}$ by diagonalizing a transfer matrix M for the partition function Z was proposed and demonstrated in Ref. 7. In this paper, we generalize the proposal of Ref. 7 to the presence of defects, focusing on topological conformal defects for concreteness. This requires several new steps, which we list here. The first two steps, which apply to generic line defects on a 2D classical partition function (equivalent to a point defect in a 1D quantum model), are: (i) encoding of the defect D as a 1D tensor network, which upon insertion in the 2D tensor network for the clean partition function Z produces a tensor network for the defect partition function Z_D as well as a tensor network for the corresponding defect transfer matrix M_D ; (ii) coarse-graining of the partition function Z_D / transfer matrix M_D . Diagonalization of the coarse-grained transfer

matrix M_D will yield the scaling dimensions Δ_α associated to defect D . Steps (i) and (ii) apply to a generic type of conformal defect. Topological conformal defects are special in that we can extract additional conformal data, namely, the conformal spins s_α , by following two additional new steps: (iii) identification of a local unitary transformation that moves the location of the topological defect, so as to be able to define a generalized translation operator T_D that commutes with the transfer matrix M_D ; (iv) coarse-graining of the generalized translation operator T_D and diagonalization of the product $T_D M_D$ of coarse-grained versions of the translation operator T_D and the transfer matrix M_D .

The main result of this paper is the proposal of the steps (i) and (iv) described above to extract accurate estimates of the $\{\Delta_\alpha, s_\alpha\}_D$ associated to a topological conformal defect, together with a thorough demonstration of the approach for the symmetry defect D_ϵ and duality defect D_σ of the critical Ising model. We also propose steps (i)-(ii) to extract accurate estimates of the Δ_α associated to a generic (i.e. non-topological) conformal defect D , which we demonstrate with specific examples.

B. Structure of this paper

Sections II–IV are mostly devoted to discussing background material, whereas Secs. V–VIII contain our main results.

In Sec. II, we review the Ising model in the absence of a defect. This includes the 2D classical Ising model on the square lattice, the 1D quantum Ising model, and the Ising CFT that effectively describes the previous two lattice models at criticality. We introduce the partition function Z and transfer matrix M , and relate the eigenvalue spectrum of M to the conformal data $\{\Delta_\alpha, s_\alpha\}$ of the three local primary fields of the Ising model. In Sec. III, we review the use of tensor networks to represent the partition function Z and transfer matrix M , and of coarse-graining algorithms for tensor networks, which allow us to obtain estimates of $\{\Delta_\alpha, s_\alpha\}$ with smaller finite-size errors than is possible with exact diagonalization. In Sec. IV, we review the properties of the topological defects D_ϵ and D_σ of the critical Ising model, including their associated field content and their fusion rules.

Sections V and VI analyze the symmetry defect D_ϵ and the duality defect D_σ , respectively. On the lattice, the topological character of a defect appears to be related to the existence of a local unitary transformation that changes the location of the defect. We identify such local unitary transformations for D_ϵ and D_σ , which also allow us to fuse these defects and confirm the expected fusion rules. We express the partition functions Z_{D_ϵ} and Z_{D_σ} of the critical Ising model in terms of transfer matrices M_{D_ϵ} and M_{D_σ} , and propose generalized translation operators T_{D_ϵ} and T_{D_σ} , which commute with M_{D_ϵ} and M_{D_σ} , respectively. Working with a tensor network representation of all the above objects, we then consider a

coarse-graining transformation for the products $M_{D_\epsilon} T_{D_\epsilon}$ and $M_{D_\sigma} T_{D_\sigma}$, whose eigenvalue spectra yield the conformal data $\{\Delta_\alpha, s_\alpha\}_{D_\epsilon}$ and $\{\Delta_\alpha, s_\alpha\}_{D_\sigma}$.

It turns out that, from a tensor network perspective, the two topological conformal defects of the Ising model are very different. Indeed, as we will see in Sec. V, the symmetry defect D_ϵ can be readily incorporated into a tensor network by employing \mathbb{Z}_2 -symmetric tensors⁸, in which case D_ϵ is represented by a simple unitary matrix V acting on a bond index. This implies, in particular, that the defect transfer matrix M_{D_ϵ} and translation operator T_{D_ϵ} are obtained from the clean transfer matrix M and translation operator T by insertions of V . This also applies to the coarse-grained version of M_{D_ϵ} and T_{D_ϵ} , and we conclude that one can extract the new set of $\{\Delta_\alpha, s_\alpha\}_{D_\epsilon}$ with remarkably little effort by recycling the coarse-grained tensor networks used for the critical Ising model without a defect. On the other hand, we will see in Sec. VI that representing the duality defect D_σ requires using different tensors altogether (as does a generic conformal defect), which one needs to explicitly coarse-grain.

In Sec. VII we then briefly discuss the case of a generic (i.e. non-topological) conformal defect D , for which we can also extract the scaling dimensions $\{\Delta_\alpha\}_D$ by diagonalizing a transfer matrix M_D for the defect partition function Z_D , and demonstrate the performance of the approach for a known continuous family of conformal defects of the critical Ising model.

Section VIII concludes the paper with a discussion of the present tensor network approach, including its extension to defects in other critical lattice models, a discussion of different coarse-graining transformations one can use, and a comparison to other tensor network approaches (based on explicitly realizing scale invariance of the tensor network under coarse-graining) that can also be used to extract conformal data. Finally, several appendices contain technical discussions, as well as a study of the \mathbb{Z}_3 symmetry defects of the three-level Potts model.

C. Source code

The numerical results we present were obtained using a Python 3 implementation of the algorithms we describe. The source code is available at <https://arxiv.org/src/1512.03846/anc>, licensed under the MIT License, a permissive free software license. It can be used to reproduce our results and as the ultimate reference on details of the algorithms we describe here.

II. CRITICAL ISING MODEL

In this section, we review the critical Ising model on the lattice, both the 2D classical partition function and the 1D quantum spin chain. We also review their continuum limit,

the Ising conformal field theory. Universal properties of the phase transition (conformal data) can be numerically estimated using exact diagonalization. The accuracy of these numerical estimates is limited by non-universal, finite-size corrections.

A. Classical partition function

The classical Ising model is defined by its Hamiltonian $K = -\sum_{\langle i,j \rangle} \sigma_i \sigma_j$, where i and j label sites on the lattice and σ_i is a classical spin variable on site i that can take the values ± 1 . $\sum_{\langle i,j \rangle}$ is a sum over nearest-neighbor pairs of sites. The partition function at inverse temperature β is

$$Z = \sum_{\{\sigma\}} e^{-\beta K} = \sum_{\{\sigma\}} e^{\beta \sum_{\langle i,j \rangle} \sigma_i \sigma_j}, \quad (1)$$

where $\sum_{\{\sigma\}}$ is a sum over all the spin configurations. Here, we consider that the spins inhabit the sites of a square lattice with periodic boundaries in both directions (a torus). The Ising Hamiltonian K is invariant under a simultaneous flip of all the spins so that if we map $\sigma_i \mapsto -\sigma_i$ for all sites i the Hamiltonian remains unchanged: $K \mapsto K$. Flipping a spin twice recovers the original configuration, so the spin-flip symmetry is a global, internal \mathbb{Z}_2 symmetry. This symmetry is preserved at high temperatures (low β) and spontaneously broken at low temperatures (large β). At $\beta = \frac{1}{2} \log(1 + \sqrt{2})$ there is a second-order phase transition that separates the low temperature symmetry-breaking, ordered phase from the high temperature disordered phase.

The Ising model on the square lattice also has a order-disorder duality called the Kramers-Wannier duality which states that a low temperature Ising model is equivalent to a high temperature model on the dual lattice. At the critical point, the model is self-dual under this duality map.⁹

On a torus made of $m \times n$ spins we can write down a transfer matrix M such that $Z = \text{Tr}(M^m)$. The transfer matrix M (which is made of $2^n \times 2^n$ entries) is associated to a row of n spins. Many questions about the model can be answered in terms of the eigenvalue spectrum of M . We omit here the explicit form of M , which we will later build using tensor networks.

B. Quantum spin chain

The one-dimensional quantum Ising model is defined by the Hamiltonian

$$H(h) = - \left(\sum_{i=1}^n \sigma_i^z \sigma_{i+1}^z + h \sum_{i=1}^n \sigma_i^x \right). \quad (2)$$

On every site i there is a quantum spin and σ^z and σ^x are Pauli matrices. The parameter h is the strength of a transverse field.

The Hamiltonian is symmetric under a global spin-flip or, in other words,

$$\Sigma^x H (\Sigma^x)^\dagger = H, \quad (3)$$

where $\Sigma^x = \bigotimes_{i=1}^n \sigma_i^x$, and there are again two phases: a symmetry-breaking phase for small transverse magnetic field, and a disordered phase for large magnetic field, with a continuous quantum phase transition at $h = 1$.

The Kramers-Wannier duality for the quantum model equates it with another spin chain living on the dual lattice with a similar Hamiltonian but with external field¹⁰ $\tilde{h} = \frac{1}{h}$. As in the classical model, the spin chain is Kramers-Wannier self-dual at the critical point.

The partition function of the quantum model for inverse temperature β_Q is $Z_Q = \text{Tr}(e^{-\beta_Q H})$. A transfer matrix for this partition function can be written as $M_Q \equiv e^{-\frac{\beta_Q}{m} H}$, so that $Z_Q = \text{Tr}((M_Q)^m)$. Through the standard classical-quantum mapping, M_Q also corresponds to a transfer matrix for the partition function of a classical two-dimensional Ising model¹¹. However, this classical dual is not the isotropic Ising model that we discussed above, but an extremely anisotropic one with very different couplings in different directions. The anisotropic and isotropic classical models are, nevertheless, in the same universality class, and hence the universal properties of the quantum and the classical Ising models are the same. To extract these universal properties we will mostly concentrate on studying the classical model.

C. Ising CFT

As we have mentioned above, the classical square lattice Ising model has a critical point at $\beta = \frac{1}{2} \log(1 + \sqrt{2})$ and the Ising spin chain has a quantum critical point at $h = 1$. The continuum limits of both of these critical points are described by the Ising CFT. The universal properties of the phase transition are captured by the conformal data of this CFT.

Consider the torus formed by parameterizing the two coordinates (x, y) of the plane by a complex variable $w \equiv x + iy$ and by identifying the points w , $w + 2\pi$ and $w + 2\pi\tau$, for $\tau = \tau_1 + i\tau_2$ a complex *modular parameter* that defines the shape of the torus. A purely imaginary modular parameter $\tau = i\tau_2$ produces a torus consisting of a rectangle with periodic boundaries.

On a torus defined by a complex modular parameter τ , the partition function of a CFT is

$$\begin{aligned} Z_{\text{CFT}} &= \text{Tr} \left(e^{-2\pi\tau_2(L_0 + \bar{L}_0 - \frac{c}{12})} e^{2\pi i\tau_1(L_0 - \bar{L}_0)} \right) \\ &= \text{Tr} \left(e^{-2\pi\tau_2 H_{\text{CFT}}} e^{2\pi i\tau_1 P} \right). \end{aligned} \quad (4)$$

Here L_0 and \bar{L}_0 are the Virasoro generators and $H_{\text{CFT}} = L_0 + \bar{L}_0 - \frac{c}{12}$ and $P = L_0 - \bar{L}_0$ are the Hamiltonian and momentum operators that generate translations in the directions $\text{Im}(w)$ and $\text{Re}(w)$, respectively, while c is the central charge.¹²

The scaling operators ϕ_α of the CFT are eigenoperators of dilations on an infinite plane. The operator-state correspondence identifies them with states $|\phi_\alpha\rangle$ that are the eigenstates of L_0 and \bar{L}_0 : $L_0|\phi_\alpha\rangle = h_\alpha|\phi_\alpha\rangle$ and $\bar{L}_0|\phi_\alpha\rangle = \bar{h}_\alpha|\phi_\alpha\rangle$. h_α and \bar{h}_α are known as the holomorphic and antiholomorphic conformal dimensions of ϕ_α . In terms of the eigenvalues of L_0 and \bar{L}_0 we can rewrite the partition function as

$$Z_{\text{CFT}} = \sum_{\alpha} e^{-2\pi\tau_2(h_\alpha + \bar{h}_\alpha - \frac{c}{12}) + 2\pi i\tau_1(h_\alpha - \bar{h}_\alpha)}, \quad (5)$$

$$= \sum_{\alpha} e^{-2\pi\tau_2(\Delta_\alpha - \frac{c}{12}) + 2\pi i\tau_1 s_\alpha}, \quad (6)$$

where $\Delta_\alpha = h_\alpha + \bar{h}_\alpha$ and $s_\alpha = h_\alpha - \bar{h}_\alpha$ are known as the scaling dimension and conformal spin of ϕ_α , respectively.¹² The scaling operators come in conformal towers built up from the primary operators. If h_p and \bar{h}_p are the conformal dimensions of a primary operator, then the scaling operators in its conformal tower have conformal dimensions of the form $h = h_p + k$ and $\bar{h} = \bar{h}_p + l$, where $k, l \in \mathbb{N}$.¹²

The Ising CFT is a conformal field theory of central charge $c = \frac{1}{2}$. For a unitary $c = \frac{1}{2}$ CFT the conformal dimensions h and \bar{h} of the primaries can take the values 0, $\frac{1}{2}$ and $\frac{1}{16}$.² However, not all the possible combinations of these values of h and \bar{h} are realized as local primary operators in the CFT. The Ising CFT only includes the three “diagonal” primary operators that have $h = \bar{h}$. They are called the identity $\mathbb{1}$ for $(0, 0)$, the energy density ϵ for $(\frac{1}{2}, \frac{1}{2})$ and the spin σ for $(\frac{1}{16}, \frac{1}{16})$. Because of the \mathbb{Z}_2 symmetry of the model, the conformal towers come with a parity (a \mathbb{Z}_2 charge). This parity is +1 for $\mathbb{1}$ and ϵ , and -1 for σ .

We will see later in Sec. IV that the non-diagonal combinations of h and \bar{h} are relevant to the discussion of topological conformal defects of the Ising CFT.

D. Extracting the universal data

For a critical, classical lattice model that has a CFT as its continuum limit, the partition function on an $m \times n$ torus (corresponding to $\tau = i\frac{m}{n}$) can be written as¹³

$$Z = \sum_{\alpha} e^{2\pi\frac{m}{n}(\frac{c}{12} - \Delta_\alpha) + mn f + \mathcal{O}(\frac{m}{n^\gamma})}, \quad \gamma > 1. \quad (7)$$

The sum is again over scaling operators. Equation (7) only differs from Eq. (5) in two non-universal terms. One non-universal term is the free energy term $mn f$, where f is the free energy per site at the thermodynamic limit. The second is the subleading finite-size corrections $\mathcal{O}(\frac{m}{n^\gamma})$, which become negligible for a large torus. The transfer matrix M corresponding to a row of n sites of the lattice so that $Z = \text{Tr}(M^m)$ then has eigenvalues¹³

$$\lambda_\alpha = e^{2\pi\frac{1}{n}(\frac{c}{12} - \Delta_\alpha) + n f + \mathcal{O}(\frac{1}{n^\gamma})}. \quad (8)$$

More generally, if the transfer matrix M corresponds instead to l rows of n sites, so that now $Z = \text{Tr}(M^{\frac{n}{l}})$, then its eigenvalues are¹³

$$\lambda_\alpha = e^{2\pi \frac{l}{n} (\frac{c}{12} - \Delta_\alpha) + l n f + \mathcal{O}(\frac{1}{n^\gamma})}. \quad (9)$$

Thus, if we manage to diagonalize a transfer matrix for large n , the subleading, non-universal corrections will become negligible, whereas we can extract f by varying l and n while keeping $\frac{l}{n}$ fixed. We can then rescale M by $e^{l n f}$ (or equivalently we can rescale the Boltzmann weights $e^{\beta \sigma_i \sigma_j}$ in the partition function Z) to get rid of the free energy term in the eigenvalue spectrum. From now on we will always assume the transfer matrix M has been rescaled in this way, so that its spectrum is

$$\lambda_\alpha \approx e^{2\pi \frac{l}{n} (\frac{c}{12} - \Delta_\alpha)}. \quad (10)$$

The equality is approximate because we have left out the subleading, non-universal, finite-size terms. Each of the eigenvalues λ_α then tells us the value of $\frac{c}{12} - \Delta_\alpha$ for one of the scaling operators ϕ_α . The scaling dimension $\Delta_{\mathbb{I}}$ of the identity operator is always 0 and for a unitary CFT this is the smallest scaling dimension possible. Thus we can obtain c from the largest eigenvalue λ_0 and the rest of the λ_α 's give us the rest of the scaling dimensions.¹⁴

For a critical quantum spin chain of n spins the spectrum of the Hamiltonian is¹³

$$E_\alpha = a + b \left[2\pi \frac{1}{n} \left(\frac{c}{12} - \Delta_\alpha \right) + n f + \mathcal{O} \left(\frac{1}{n^\gamma} \right) \right] \quad (11)$$

where a and b are non-universal constants and $\gamma > 1$ as before. We could thus extract all the same critical data by diagonalizing the quantum Hamiltonian H instead of the transfer matrix M of the classical partition function Z . In this work we choose, however, to work mostly with the transfer matrix.

For a translationally invariant lattice model, such as the Ising model, the transfer matrix M commutes with the translation operator $T = e^{\frac{2\pi i}{n} P}$ that implements a discrete translation by one lattice site. Each eigenstate of T , with eigenvalue $e^{\frac{2\pi i}{n} p_\alpha}$, has well-defined momentum p_α . As discussed above, the momentum operator is $P = L_0 - \bar{L}_0$ and thus the momentum p_α corresponds to a conformal spin $s_\alpha = h - \bar{h}$. Hence we can diagonalize T and M simultaneously to obtain both the scaling dimensions Δ_α and the conformal spins s_α for the scaling operators ϕ_α . In fact, we can get away with even less work by diagonalizing only the product $T \cdot M$, which corresponds to the transfer matrix on a torus with a modular parameter τ that has real part $\tau_1 = \text{Re}(\tau) = 1/n$ and imaginary part $\tau_2 = \text{Im}(\tau) = l/n$. The eigenvalues of $T \cdot M$ are the products of the eigenvalues of T and M ,

$$\tilde{\lambda}_\alpha = \lambda_\alpha \cdot e^{\frac{2\pi i}{n} p_\alpha} \approx e^{2\pi \frac{l}{n} (\frac{c}{12} - \Delta_\alpha) + \frac{2\pi i}{n} s_\alpha}, \quad (12)$$

where we have again scaled away the free energy contribution and ignored the subleading finite-size corrections. The real part $\text{Re}(\log \tilde{\lambda}_\alpha) = 2\pi \frac{l}{n} (\frac{c}{12} - \Delta_\alpha)$ then

yields the scaling dimension Δ_α and the imaginary part $\text{Im}(\log \tilde{\lambda}_\alpha) = \frac{2\pi i}{n} s_\alpha$ the conformal spin s_α . Note that because of the periodicity of $e^{\frac{2\pi i}{n} s_\alpha}$, the spin can only be determined modulo n , a point we will come back to later.

Thus to obtain scaling dimensions and conformal spins $\{\Delta_\alpha, s_\alpha\}$ of the CFT numerically we can construct $T \cdot M$ for a finite but sufficiently large system and diagonalize it using an exact diagonalization algorithm. Results obtained in this manner are shown in Fig. 2. They clearly show the structure of the conformal towers coming out correctly and the accuracy of the estimates of Δ_α for the operators with lowest scaling dimensions is remarkably good. However, for operators with higher scaling dimensions the numerical estimates start to deteriorate significantly. This is due to the subleading finite-size corrections, which are still large at the system size $n = 18$ that we used here.

Unfortunately if we try to push for larger systems the computations quickly become prohibitively expensive because the dimension of the transfer matrix grows as 2^n and the cost of exact diagonalization grows as the third power of this dimension. To diminish the effect of these non-universal corrections, we can describe the system using tensor networks and apply tensor network coarse-graining algorithms to reach large system sizes, as we review in the next section.

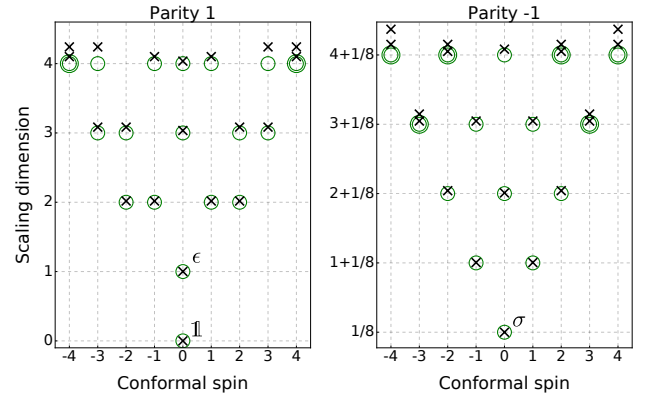


Figure 2. The scaling dimensions (vertical axis) and conformal spins (horizontal axis) of the first scaling operators of the Ising CFT obtained from exact diagonalization of a transfer matrix of $n = 18$ sites. The scaling operators are divided by their parity, i.e. their eigenvalue under the \mathbb{Z}_2 symmetry operator Σ^x that commutes with the transfer matrix. The crosses mark the numerical values that can be compared with the circles that are centered at the exact values. Several concentric circles denote the degeneracy N_α of that $(\Delta_\alpha, s_\alpha)$ pair. The primary fields *identity* \mathbb{I} , *spin* σ and *energy density* ϵ appear at the basis of their three conformal towers.

III. TENSOR NETWORKS

In this section, we first review how tensor networks can be used to express the partition function Z and its trans-

fer matrix M . We then describe how a coarse-graining algorithm for tensor networks can be used to analyze larger systems than with exact diagonalization, as first proposed and demonstrated in Ref. 7. By diagonalizing a transfer matrix M corresponding to a large number n of sites we can reduce very significantly the errors, due to finite-size corrections, in the estimates of scaling dimensions and conformal spins $\{\Delta_\alpha, s_\alpha\}$. This comes at the price of introducing truncation errors.

A. Tensor network representation

In terms of the Boltzmann weights $B_{ij} = e^{\beta\sigma_i\sigma_j}$ the partition function is

$$Z = \sum_{\{\sigma\}} \prod_{\langle i,j \rangle} B_{ij}, \quad (13)$$

with the sum and the product being over all spin configurations and all nearest-neighbor pairs, respectively. Periodic boundary conditions in both directions are again assumed. Such a partition function Z can be written as a tensor network in several ways. We will be using the network shown in Fig. 3(a) on the right. The first network in Fig. 3(a) is a straight-forward translation of Eq. (13) into the graphical tensor network notation. In it for every spin there is a four-index Kronecker delta δ_{ijkl} . Each of the four indices connects to one of the neighboring spins through the matrix B . On the right this is then rewritten in terms of tensor $A_{ijkl} = B_{ij}B_{jk}B_{kl}B_{li}$ that encodes the interactions around a plaquette of spins. Every index of A corresponds to one spin. We will be working with this latter network, which we denote $Z_{n,m}(A)$. Notice that here m and n label the number of rows and columns of tensors A , not of spins, with each tensor accounting for two spins. However, all the expressions in the preceding section can be seen to remain valid due to the isotropy of the original spin model. We also note that, alternatively, one can build a single tensor A for each spin following the construction in Ref. 15.

From Fig. 3(a) it is clear that we can write $Z = \text{Tr}(M^m)$ where the transfer matrix is as in Fig. 3(b), or in other words

$$M_{j_1 j_2 \dots j_n}^{k_1 k_2 \dots k_n} = \sum_{i_1, i_2, \dots, i_n} \prod_{\alpha=1}^n A_{i_\alpha j_\alpha i_{\alpha+1} k_\alpha}. \quad (14)$$

Here all the i_α indices are summed over and i_{n+1} is identified with i_1 . When writing $\text{Tr}(M^m)$ we have interpreted M as a linear map from \mathbb{V}_j to \mathbb{V}_k , where \mathbb{V}_j (respectively \mathbb{V}_k) is the tensor product of the vector spaces of the indices j_α (respectively k_α).

Implementing a lattice translation in the network is straight-forward, and shown in Fig. 3(c). In Fig. 3(d) is the operator $T \cdot M$, which we want to diagonalize in order to extract universal data of a phase transition (see previous section).

It should be noted here that when we translate between network diagrams and equations, our convention is that reading an equation from left to right corresponds to reading a diagram from either left to right or bottom to top, but never right to left or top to bottom.

The \mathbb{Z}_2 symmetry of the Ising model plays an important role in the tensor network representation, as we will see later when we consider a system with a topological defect. For a model with a global internal symmetry, the symmetry can be made manifest in the tensors themselves. This is covered in length in Refs. 8, 16, and 17. For the present discussion it suffices to know that for the Ising model, we use tensors that fulfill the identity in Fig. 4, namely, tensors that are left unchanged if we apply a spin-flip matrix V on each of the indices. The spin-flip matrix V here is nothing but σ^x , but we call it V for consistency with the case where it acts on a coarse-grained index. As explained in Appendix A, in general V is some unitary representation of the non-trivial element of the symmetry group \mathbb{Z}_2 . In other words it is a unitary matrix such that $V^2 = \mathbb{1}$. We call a tensor that obeys the invariance property of Fig. 4 a \mathbb{Z}_2 invariant tensor. The vector space attached to each index of a \mathbb{Z}_2 invariant tensor can be understood as the direct sum of two subspaces, one for each parity \pm (i.e. each \mathbb{Z}_2 charge). In this way, we can attach a parity to each eigenvalue/vector of the transfer matrix and, by extension, to the corresponding scaling operators ϕ_α (discussed in the previous section).

B. Coarse-graining

A tensor network coarse-graining transformation maps a network like $Z_{n,m}(A)$ [see Fig. 3(a)] to a smaller network $Z_{n',m'}(A')$ that is of the same form but consists of tensors A' . Each A' corresponds to a small region of the original network $Z_{n,m}(A)$ and describes longer length scale features of the system. For concreteness we consider a coarse-graining where each A' corresponds to four of the original tensors A and $n' = \frac{n}{2}$ and $m' = \frac{m}{2}$, i.e. the coarse-graining has scaled the linear size of the system by a factor of $\frac{1}{2}$.

Ideally, this coarse-graining would be such that the original network $Z_{n,m}(A)$ and the coarse-grained $Z_{\frac{n}{2}, \frac{m}{2}}(A')$ would contract to exactly the same value: the partition function Z . In practice small errors, called truncation errors, need to be introduced to keep the computational cost from growing too large, and thus the two networks contract to only approximately the same value.

We can use such a coarse-graining repeatedly to produce a series of tensors $A^{(0)} \mapsto A^{(1)} \mapsto \dots \mapsto A^{(s)}$ such that $A^{(0)} \equiv A$ and each $A^{(s)}$ represents 4^s of the original tensors $A^{(0)}$. For each tensor $A^{(s)}$ the network $Z_{\frac{n}{2^s}, \frac{m}{2^s}}(A^{(s)})$ is an approximate representation of the original network $Z_{n,m}(A^{(0)})$. This is illustrated in Fig. 5. As first proposed and demonstrated in Ref. 7, we can then use the coarse-grained tensors $A^{(s)}$ to produce a transfer matrix M representing many spins and extract $\{\Delta_\alpha, s_\alpha\}$ with

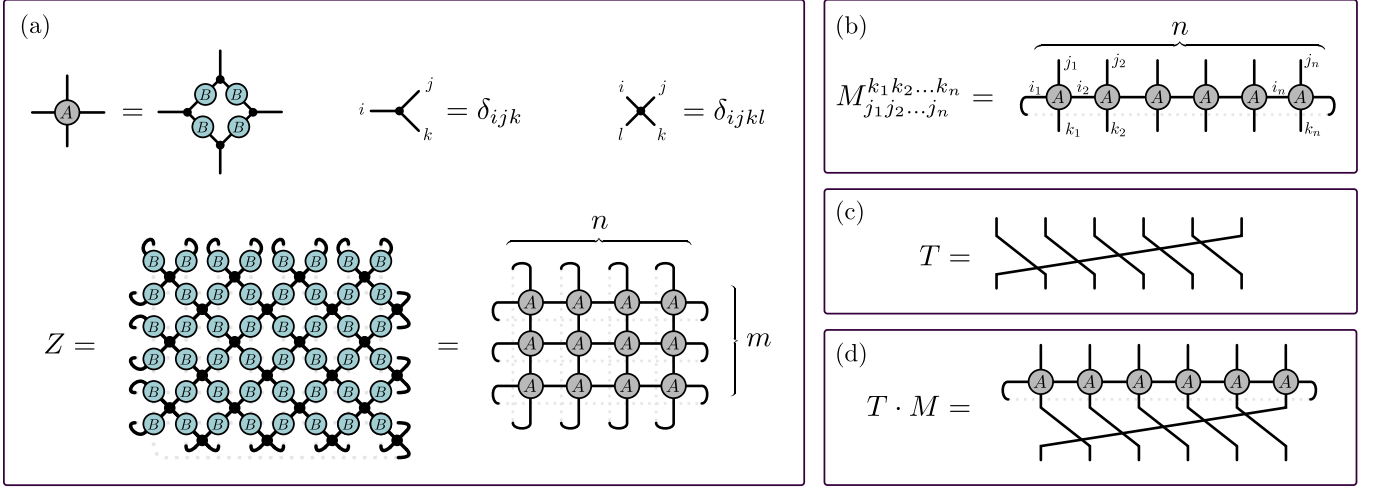


Figure 3. In this figure and throughout the paper we use the usual graphical tensor network language where tensors are represented by various shapes and their indices by legs coming out from them. A leg connecting two tensors is summed over. (a) The partition function Z of a classical two dimensional lattice model on a torus as a tensor network, first using the Boltzmann weights $B_{ij} = e^{-\beta E_{ij}}$ and then in terms of the tensor $A_{ijkl} = B_{ij}B_{jk}B_{kl}B_{li}$. We call the network on the right $Z_{n,m}(A)$. δ_{ijk} and δ_{ijkl} are three- and four-way Kronecker deltas that fix all their indices to have the same value. (b) The transfer matrix M as a tensor network. (c) The one-site translation operator T . (d) The translation operator composed with the transfer matrix.

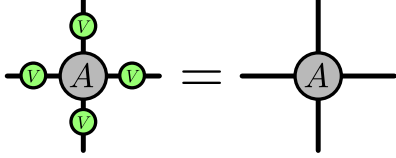


Figure 4. The invariance of tensor A under the symmetry transformation V .

smaller finite-size corrections. We emphasize that although Ref. 7 described this approach in the context of a particular coarse-graining scheme, namely the *tensor entanglement-filtering renormalization* (TEFR) method, it can be used with any coarse-graining scheme that accurately preserves the partition function Z or transfer matrix M .

A key role in any coarse-graining scheme is played by the dimension χ of the indices of $A^{(s)}$, called the bond dimension of the network. The bond dimension controls both the computational cost of the coarse-graining, which grows as a power of χ , and the truncation errors introduced at each coarse-graining step, which decrease with growing χ . For the purpose of estimating $\{\Delta_\alpha, s_\alpha\}$, a useful coarse-graining scheme is then one where a sufficiently small χ (leading to a sufficiently small computational cost) can be kept over several coarse-graining steps (so that large system sizes can be considered, reducing the finite-size corrections) while at the same time keeping the truncation errors sufficiently small, so that they do not significantly affect the numerical estimates. Thus, for a fixed bond dimension χ (that is, for a fixed computational cost per coarse-graining step), the best numerical estimates are obtained by applying a number of iterations s

such that the finite-size corrections and truncation errors are of the same magnitude, and their cumulative effect on the results is at a minimum.

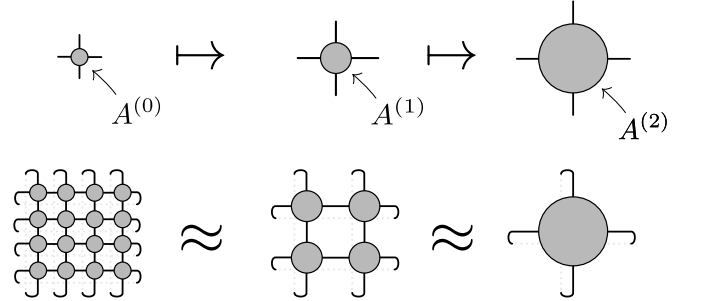


Figure 5. Repeating a coarse-graining produces a series of tensors $A^{(s)}$ and corresponding networks that all contract to approximately the same value. We think of each $A^{(s)}$ as representing a local patch of the system at a different length scale. With a $2 \times 2 \mapsto 1$ coarse-graining like the one we consider, a network $Z_{2^k, 2^k}(A)$ can be coarse-grained to a single tensor in k steps.

The specific coarse-graining scheme that we use in this paper is called *tensor network renormalization* (TNR)¹⁸. It is based on inserting approximate partitions of unity into the network, consisting of isometric and unitary tensors, that can be optimized to minimize the truncation error. We will not explain the details of the algorithm in this paper, but refer the reader to Refs. 19 and 18. However, an outline of the algorithm can be found in Appendix A. Similar results to the ones obtained in this paper with TNR could equally well be obtained (perhaps with less accuracy or increased computational cost) using any coarse-graining that acts sufficiently locally, such

as the simpler tensor renormalization group algorithm²⁰. This point is elaborated further in the discussion section.

Applying a $2 \times 2 \mapsto 1$ coarse-graining transformation s times, a transfer matrix of $2^s \times (2^s \cdot n_s)$ tensors A can be coarse-grained down to the transfer matrix $M^{(s)}$ in Fig. 6, consisting of a row of n_s tensors $A^{(s)}$. The computational cost thus scales logarithmically in system size. Interpreted as a matrix, $M^{(s)}$ has dimensions $\chi^{n_s} \times \chi^{n_s}$, and can be diagonalized for sufficiently small values of n_s and χ . We diagonalize $M^{(s)}$ simultaneously with a translation operator $T^{(s)}$, also shown in Fig. 6. $T^{(s)}$ is a translation by 2^s sites in the original system and its eigenvalues yield the conformal spins modulo n_s , as explained in Appendix A. In Appendix B we show how to perform a final coarse-graining step on the composite operator $T^{(s)} \cdot M^{(s)}$ to raise the periodicity of the conformal spins to $2n_s$.

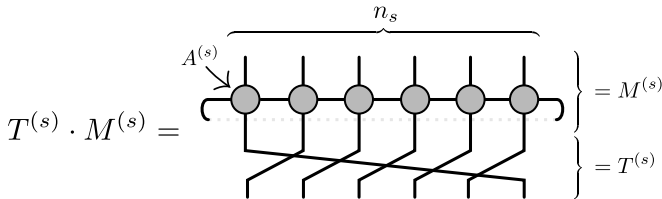


Figure 6. The coarse-grained transfer matrix and translation operator.

C. Numerical results

In Fig. 7, we show scaling dimensions and conformal spins $\{\Delta_\alpha, s_\alpha\}$ obtained by diagonalizing a transfer matrix that has been coarse-grained using TNR. To obtain the scaling dimensions we have coarse-grained a transfer matrix of 4 tensors $A^{(s)}$ for $s = 7$ (corresponding to $2 \times 4 \times 2^7 \times 2^7 = 2^{17} \approx 130\,000$ spins) using bond dimensions $\chi' = 14$ and $\chi = 28$ (the TNR scheme we use has two relevant bond dimensions, see Appendix A). For the conformal spins a slightly larger system was used, as explained in Appendix B. The numerical results are in excellent agreement with the exact values even higher up in the conformal towers, in contrast with the exact diagonalization results in Fig. 2. Table I shows a comparison of the numerical values to the exact ones for the primary fields. For the central charge we obtain $c = 0.500091$ where the exact value would be $\frac{1}{2}$.

D. Multi-scale entanglement renormalization ansatz

We conclude this section by recalling that, as explained in Ref. 21, if we apply TNR to a tensor network representing the Euclidean path integral $e^{-\beta_Q H}$ of a quantum Hamiltonian H , we obtain a multi-scale entanglement renormalization ansatz (MERA) for the ground state of H . Such a MERA, shown in Fig. 8, is built of tensors

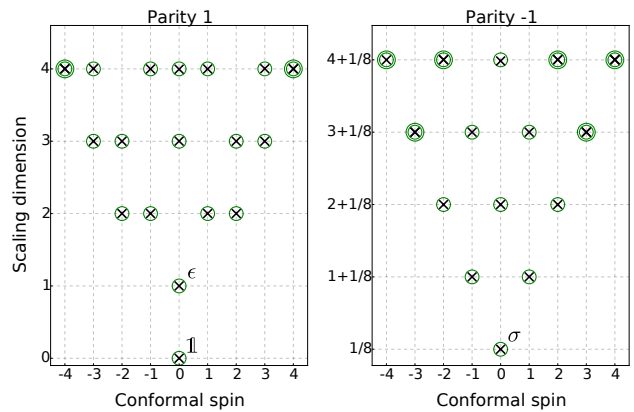


Figure 7. By coarse-graining and diagonalizing a transfer matrix for the classical square lattice Ising model we have obtained scaling dimensions (vertical axis) and conformal spins (horizontal axis) of the first few scaling operators with lowest dimensions in the Ising CFT. The crosses mark the numerical values that should be compared with the circles that are centered at the exact values. The scaling operators are divided according to their \mathbb{Z}_2 charge, that is their parity under a global spin-flip. Several concentric circles denote the degeneracy N_α of that $(\Delta_\alpha, s_\alpha)$ pair. Although it is not clear from the figure, these degeneracies also come out correctly.

Primary	(h, \bar{h})	Δ_{TNR}	Δ_{exact}	s_{TNR}	s_{exact}
$\mathbb{1}$	$(0, 0)$	—	0	0	0
ϵ	$(1/2, 1/2)$	1.000256	1	0	0
σ	$(1/16, 1/16)$	0.125109	0.125	0	0

Table I. The scaling dimensions and conformal spins of the primary fields of the Ising CFT obtained using TNR, contrasted with the exact values. No numerical value for the scaling dimension of the identity operator is provided because we extract the central charge c by assuming that $\Delta_{\mathbb{1}} = 0$ exactly. The central charge we get is $c = 0.500091$ whereas the exact one is $c = \frac{1}{2}$. The conformal spins we obtain are exactly zero without any numerical errors, because we know that the possible eigenvalues of the translation operator for a four site system are ± 1 and $\pm i$, which yields the possible conformal spins $-1, 0, 1$ and 2 .

(called disentanglers and isometries) that are produced during the coarse-graining of the Euclidean path integral. We have observed empirically that the partition function of the 2D classical Ising model that we study is also the Euclidean path integral of the 1D quantum model. It then follows that the disentanglers and isometries produced during the coarse-graining of the classical partition function Z can be put together into a MERA that represents the ground state of the Hamiltonian H for the 1D quantum Ising model. This observation will extend to the case of topological defects, discussed in Secs. V and VI.

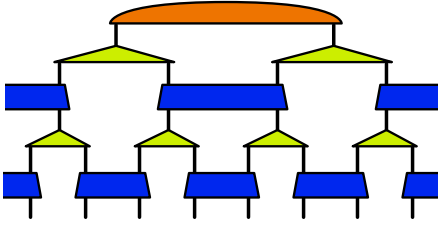


Figure 8. A MERA for a state of eight spins in a system with periodic boundaries. Such a network for the ground state of a spin chain can be obtained by applying TNR to a tensor network describing the Euclidean path integral of the quantum Hamiltonian²¹. The tensors in the network are the same unitaries and isometries as used in Appendix A. Even though our notation does not reflect it, the unitaries and isometries on different layers generally differ from each other.

IV. TOPOLOGICAL DEFECTS

In this section, we review the topological conformal defects (often referred to simply as topological defects) of the Ising CFT. On a torus these defects can be thought of as different boundary conditions, and their presence modifies the operator content of the partition function. The Ising CFT has two different non-trivial topological defects, which we introduce in this section and whose lattice realization will be analyzed in the next two sections.

As stated earlier in Eq. (4), the partition function of a CFT on a torus can be written as

$$Z_{\text{CFT}} = \text{Tr} (e^{-2\pi\tau_2 H_{\text{CFT}}} e^{2\pi i\tau_1 P}). \quad (15)$$

We consider now a twisted partition function Z_D of the form²²

$$Z_D = \text{Tr} (D e^{-2\pi\tau_2 H_{\text{CFT}}} e^{2\pi i\tau_1 P}). \quad (16)$$

D is the twist operator, which can be thought of as implementing a special type of boundary condition on the torus. If D commutes with all the generators of the Virasoro algebra it is called a topological conformal defect (topological defect for simplicity). A twist operator can be seen as a line defect that loops around the torus. If the defect is topological the loop can be freely deformed without affecting correlation functions in the system as long as the defect is not moved across a field insertion. The conformality of the defect also means that it is invariant under scale transformations.^{6,23}

The twisted partition function Z_D for a topological defect can be written as a sum of terms corresponding to scaling dimensions and conformal spins $\{\Delta_\alpha, s_\alpha\}_D$, similarly as for the non-twisted Z in Eq. (5). However, the $\{\Delta_\alpha, s_\alpha\}_D$ present in the sum are in general different from those of the non-twisted Z .^{6,23}

For the Ising CFT, all possible topological defects can be built as linear combinations of three defects which we denote $D_{\mathbb{1}}$, D_ϵ and D_σ . They are known as the *simple* defects of the Ising CFT and are related to the same irreducible representations of the Virasoro algebra as the

primary fields $\mathbb{1}$, ϵ and σ , hence the names.^{6,24} The $D_{\mathbb{1}}$ defect is the trivial defect or rather the lack of any defect where the twist operator is just the identity. The partition function for it, $Z_{D_{\mathbb{1}}} = Z$, has been the topic of the last two sections of the paper. D_ϵ is also known as the (\mathbb{Z}_2) symmetry defect and D_σ is called the (Kramers-Wannier) duality defect.

The operators present in the twisted partition functions Z_{D_ϵ} and Z_{D_σ} come organized in conformal towers built on top of primary operators, each of which is identified with conformal dimensions (h, \bar{h}) that may take values 0 , $\frac{1}{2}$ and $\frac{1}{16}$, just like for the operators of the non-twisted $Z_{D_{\mathbb{1}}}$. The combinations of h and \bar{h} that are present in each partition function are shown in Table II. Note that together the three partition functions include all the possible pairs (h, \bar{h}) .⁶

$Z_{D_{\mathbb{1}}}$	0	$\frac{1}{2}$	$\frac{1}{16}$	Z_{D_ϵ}	0	$\frac{1}{2}$	$\frac{1}{16}$	Z_{D_σ}	0	$\frac{1}{2}$	$\frac{1}{16}$
0	$\mathbb{1}$			0	ψ			0			X
$\frac{1}{2}$		ϵ		$\frac{1}{2}$	$\bar{\psi}$			$\frac{1}{2}$			Y
$\frac{1}{16}$			σ	$\frac{1}{16}$		μ		$\frac{1}{16}$	\bar{X}	\bar{Y}	

Table II. The primary operators with conformal dimensions (h, \bar{h}) included in the Ising partition functions with different defects in them. The horizontal axis is h , the vertical one is \bar{h} . The operators in $Z_{D_{\mathbb{1}}}$ and Z_{D_ϵ} have established names shown in the table, with the $Z_{D_{\mathbb{1}}}$ ones already familiar to us from earlier in the paper. The ones included in Z_{D_σ} we denote X , \bar{X} , Y and \bar{Y} in the absence of more a established convention.

Consider bringing two defects next to each other so that they effectively behave as one defect. This gives rise to fusion rules for topological defects. The fusion rules of the topological defects of the Ising model are the same as the fusion rules of the primary operators, namely

$$D_\epsilon \times D_\epsilon = D_{\mathbb{1}} \quad (17)$$

$$D_\sigma \times D_\epsilon = D_\sigma \quad (18)$$

$$D_\sigma \times D_\sigma = D_{\mathbb{1}} + D_\epsilon. \quad (19)$$

The next two sections are devoted to analyzing the two non-trivial defects D_ϵ and D_σ on the lattice. Similarly as we have done in the two preceding sections for the trivial defect $D_{\mathbb{1}}$, we will first study the realization of each defect in the quantum and classical lattice models, then discuss how to represent them using tensor networks, and finally study how to coarse-grain these networks. We will then diagonalize transfer matrices for the twisted partition functions and extract the scaling dimensions and conformal spins of the scaling operators. In the process we will also end up discussing how these defects can be moved around and how their fusion rules manifest in the lattice models.

V. SYMMETRY DEFECT D_ϵ

In this section, we review how to realize, on the lattice, the symmetry defect D_ϵ of the Ising CFT in the

classical and quantum Ising models and present a way of implementing D_ϵ in a tensor network. We discuss how to coarse-grain this tensor network representation and use it to numerically evaluate the scaling dimensions and conformal spins $\{\Delta_\alpha, s_\alpha\}_{D_\epsilon}$ of the operators in the twisted partition function Z_{D_ϵ} .

A. Lattice representation

The symmetry defect D_ϵ is directly related to the \mathbb{Z}_2 spin-flip symmetry of the Ising model. Consider the classical Ising model on a square lattice and draw a closed loop around a connected region of spins. If one flips the spins encircled by the loop, then most of the terms $-\sigma_i\sigma_j$ in the Hamiltonian are unaffected, but along the loop there is a string of nearest-neighbor pairs where one of the spins is flipped and the other one is not and their couplings become $\sigma_i\sigma_j$. This string is the classical lattice realization of the D_ϵ defect.

We are interested in a partition function Z_{D_ϵ} where such a defect forms a non-contractible loop around a torus. Z_{D_ϵ} is said to have antiperiodic boundary conditions due to how most of the spins are coupled ferromagnetically but along the boundary the coupling is antiferromagnetic.

Analogously, in the quantum spin chain the D_ϵ defect is realized by changing the sign of one of the nearest-neighbor terms to obtain

$$H_{D_\epsilon} = - \left(\sum_{i=1}^{n-1} \sigma_i^z \sigma_{i+1}^z - \sigma_n^z \sigma_1^z + \sum_{i=1}^n \sigma_i^x \right). \quad (20)$$

Let us concentrate on the quantum case for a moment and consider moving and fusing D_ϵ defects. In the Hamiltonian 20 the defect is located on the coupling between spins n and 1. If we conjugate the Hamiltonian with σ_n^x , we effectively move the defect by one site:

$$\sigma_n^x H_{D_\epsilon} \sigma_n^x = - \left(\sum_{i=1}^{n-2} \sigma_i^z \sigma_{i+1}^z + \sum_{i=1}^n \sigma_i^x \right. \quad (21)$$

$$\left. - \sigma_{n-1}^z \sigma_n^z + \sigma_n^z \sigma_1^z \right). \quad (22)$$

σ_n^x is unitary and Hermitian and conjugating by it does not affect the spectrum of the Hamiltonian. Using σ^x to move defects one can easily check that taking a Hamiltonian with two D_ϵ defects and moving them to the same site gives the usual Ising Hamiltonian H . This is the fusion rule $D_\epsilon \times D_\epsilon = D_\mathbb{1}$.

Similarly in the classical model a D_ϵ defect can be moved by flipping a spin that is next to it. This is because flipping a spin changes all its couplings from ferromagnetic to antiferromagnetic or vice versa. Such a spin-flip is only a matter of relabeling a degree of freedom and does not affect the partition function. Now consider a system with two D_ϵ defects parallel to each other and move one of them until there is only a string of spins between the two

defects. Flipping the spins between the defects changes all the antiferromagnetic couplings to ferromagnetic and we are left with the usual Ising model — a $D_\mathbb{1}$ defect.

B. Tensor network representation

In a tensor network $Z_{n,m}(A)$ that represents a partition function $Z_{D_\mathbb{1}}$ [see Fig. 3(a)], every bond corresponds to one classical spin. If we multiply one of the legs i of a tensor A_{ijkl} with a spin-flip matrix V this makes the corresponding spin i couple antiferromagnetically to its neighbors on one side. Thus, the network for Z_{D_ϵ} is as depicted in Fig. 9(a), where the defect lives on a string of bonds. The same figure shows the transfer matrix M_{D_ϵ} for this twisted partition function.

Just as in the system without a defect, by diagonalizing M_{D_ϵ} we can extract the scaling dimensions of the operators in Z_{D_ϵ} . For the conformal spins we would need to diagonalize M_{D_ϵ} simultaneously with the translation operator. However, the usual lattice translation T does not commute with M_{D_ϵ} because the translation moves the defect by one lattice site. We can move the defect back to where it was by conjugating the tensor A that is next to the defect with V from above and below, as shown in Fig. 9(b).

Thus the operator $T_{D_\epsilon} = VT$ commutes with M_{D_ϵ} . We call T_{D_ϵ} the generalized translation operator for the D_ϵ defect. It is the notion of translation under which the partition function with a D_ϵ defect is translation invariant.^{25,26} $T_{D_\epsilon} \cdot M_{D_\epsilon}$, shown in Fig. 9(c), has a spectrum of the form in Eq. (12) from which the conformal spins and scaling dimensions of the operators in Z_{D_ϵ} can be obtained. Figure 10 shows estimates for $\{\Delta_\alpha, s_\alpha\}$ obtained numerically by diagonalizing a transfer matrix consisting of $n = 18$ tensors. The structure of the bottom of the conformal towers can be clearly recognized, but the accuracy of the estimates deteriorates quickly as we look at larger scaling dimensions. We shall see below that again increasing the system size by using a coarse-graining algorithm will greatly improve these estimates.

C. Coarse-graining

Coarse-graining the symmetry defect is trivial when we use a coarse-graining scheme that is based on using \mathbb{Z}_2 invariant tensors: By utilizing the invariance of all the tensors involved we can move the string of spin-flip matrices V to the next scale without any additional numerical effort. In other words, as is shown in Fig. 11, a network $Z_{n,m}(A)$ that has V matrices on a string of bonds coarse-grains into a network $Z_{\frac{n}{2}, \frac{m}{2}}(A')$ with matrices V' on a string of bonds. A' is the same tensor that we obtain when coarse-graining a network without a defect. V' 's are the spin-flip matrices of the bonds of the coarse-grained network, i.e. the unitary representations of the non-trivial element of \mathbb{Z}_2 under which A' is \mathbb{Z}_2 invariant. Similarly,

as for the D_1 case: A transfer matrix of $2^7 \times (4 \times 2^7)$ tensors $A^{(0)}$ (corresponding to $2 \times 4 \times 2^7 \times 2^7 = 2^{17}$ spins) coarse-grained with bond dimensions $\chi' = 14$ and $\chi = 28$ for the scaling dimensions and a transfer matrix twice as wide and with one additional coarse-graining step for the conformal spins, as explained in Appendix B.

Primary	(h, \bar{h})	Δ_{TNR}	Δ_{exact}	s_{TNR}	s_{exact}
μ	$(1/16, 1/16)$	0.1249287	0.125	10^{-16}	0
ψ	$(1/2, 0)$	0.5000704	0.5	0.4999847	0.5
$\bar{\psi}$	$(0, 1/2)$	0.5000704	0.5	-0.4999847	-0.5

Table III. The scaling dimensions Δ and conformal spins s for the primaries of Z_{D_ϵ} as obtained with TNR compared with the exact values. Note that one could easily see that the conformal spins must be half-integers in the parity -1 sector and integers in the parity $+1$ sector by observing that $(T_{D_\epsilon})^n = \Sigma^x$, the \mathbb{Z}_2 symmetry operator. However, we choose to present the numerical values for the conformal spins, including the small numerical errors, to demonstrate the accuracy of our method.

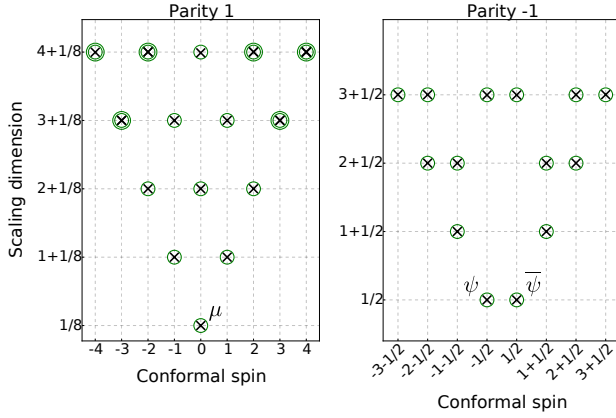


Figure 12. The scaling dimensions (vertical axis) and conformal spins (horizontal axis) of the first scaling operators of the two-dimensional classical Ising model with a D_ϵ defect as obtained with TNR. The crosses mark the numerical values and the circles mark the exact values. The scaling operators are divided according to their \mathbb{Z}_2 charge, that is their parity under a global spin-flip. Several concentric circles denote the degeneracy N_α of that $(\Delta_\alpha, s_\alpha)$ pair.

E. MERA

By using TNR to coarse-grain the tensor network for Z_{D_ϵ} we get a MERA for the ground state of the quantum model with a D_ϵ defect. As shown in Fig. 13 it is like the defectless MERA, but with a spin-flip matrix $V^{(s)}$ at every layer and a different top tensor. Note that this is a special case of an impurity MERA, discussed in Ref. 27.

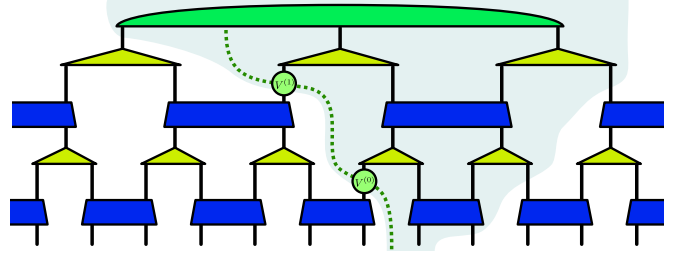


Figure 13. A MERA for the ground state of the quantum spin chain that has a symmetry defect in it, produced by coarse-graining the tensor network for Z_{D_ϵ} with TNR. Compared to the MERA without a defect [Fig. 8] the only differences here are the spin-flip matrices and the different top tensor. Like the V 's, the new top tensor can also be obtained without additional numerical work. The dotted green line traces the path of the defect through the coarse-graining. Note how at every layer of the MERA the defect is situated between two sites. We could have chosen the defect to take different paths through the network by choosing slightly different coarse-graining schemes (see Appendix A for details on the scheme we use). Shown in pale blue is the causal cone of the site that is situated next to the defect. The dotted green line of the defect follows the edge of this causal cone. This is a special case of the more general situation where a defect may affect the tensors within, and only within, its causal cone. We shall encounter the more general situation in the next section, specifically in Fig. 19.

VI. DUALITY DEFECT D_σ

In this section, we first review the realization, on a quantum spin chain, of the Kramers-Wannier duality defect D_σ of the Ising CFT, and how one can move the defect with a local unitary operator. We then construct a tensor network representation of the duality defect D_σ for the classical partition function. We discuss how the defect can be coarse-grained following a strategy that is common to any type of line defect since, in contrast to the symmetry defect D_ϵ , we are not able to incorporate the duality defect D_σ into the bond index. Finally, we present numerical results for the scaling dimensions and conformal spins $\{\Delta_\alpha, s_\alpha\}_{D_\sigma}$ of the scaling operators in the twisted partition function Z_{D_σ} .

A. Lattice representation

The duality defect D_σ is related to the Kramers-Wannier self-duality of the critical Ising model in a manner similar to how the symmetry defect D_ϵ is related to the \mathbb{Z}_2 symmetry of the model. To the best of our knowledge, its explicit realization on the classical partition function was not known (although Ref. 28 reports related work). For the quantum spin chain, the D_σ defect is realized in the Hamiltonian¹⁰

$$H_{D_\sigma} = - \left(\sum_{i=1}^{n-1} \sigma_i^z \sigma_{i+1}^z + \sum_{i=1}^{n-1} \sigma_i^x + \sigma_n^y \sigma_1^z \right). \quad (23)$$

Note that, in addition to the new term involving σ^y , the one-site term σ^x is missing from the n th site. We say that in this Hamiltonian the defect is on site n .

As before for the D_ϵ defect, we need a way to move the D_σ defect from one site to the next. The quantum Ising model can be mapped to a theory of free Majorana fermions with a Jordan-Wigner transformation. In the Majorana fermion picture the D_σ defect corresponds to one fermion missing from the chain. There it is then clear what moving the defect means. Translating this back to the spin chain language gives the two-site unitary operator¹⁰ (acting here on sites 1 and n)

$$U_{D_\sigma} = \left[\left(R_z^{\frac{\pi}{4}} \right)_n \otimes \left(R_y^{\frac{\pi}{4}} R_x^{\frac{\pi}{4}} \right)_1 \right] \text{CZ}_{1,n}. \quad (24)$$

Here $R_a^\alpha = e^{i\alpha\sigma^a} = \mathbb{1} \cos(\alpha) + i\sigma^a \sin(\alpha)$ with σ^a 's being the Pauli matrices and $\text{CZ}_{1,n}$ is a controlled-Z gate $|0\rangle\langle 0|_n \otimes \mathbb{1}_1 + |1\rangle\langle 1|_n \otimes \sigma_1^z$. Which site is considered the control qubit for CZ does not matter because CZ is symmetric under swapping of the two sites. U_{D_σ} moves the defect in the sense that

$$U_{D_\sigma} H_{D_\sigma} U_{D_\sigma}^\dagger = - \left(\sum_{i=2}^n \sigma_i^z \sigma_{i+1}^z + \sum_{i=2}^n \sigma_i^x + \sigma_1^y \sigma_2^z \right) \quad (25)$$

which is like H_{D_σ} but with the defect now on site 1. We will be referring to U_{D_σ} , H_{D_σ} and $U_{D_\sigma}^\dagger$ without mentioning which site the defect is on and which sites U_{D_σ} operates on as this should be clear from the context.

Next, we briefly investigate how the fusion rules come about in the quantum Hamiltonian. We take a Hamiltonian that has a D_ϵ defect on one site and a D_σ defect on another. By moving either one (or both) of the defects by conjugating with U_{D_σ} or V we can bring both of the two defects to site n . The resulting Hamiltonian is

$$H_{D_\epsilon \times D_\sigma} = - \left(\sum_{i=1}^{n-1} \sigma_i^z \sigma_{i+1}^z + \sum_{i=1}^{n-1} \sigma_i^x - \sigma_n^y \sigma_1^z \right). \quad (26)$$

This is related to H_{D_σ} by conjugation with the unitary σ_n^z . Therefore it is the same defect D_σ up to a local change of basis, thus demonstrating the fusion rule $D_\epsilon \times D_\sigma = D_\sigma$.

Next consider a Hamiltonian with two D_σ defects on different sites, such as

$$- \left(\sum_{i \neq 1,4} \sigma_i^z \sigma_{i+1}^z + \sum_{i \neq 1,4} \sigma_i^x + \sigma_1^y \sigma_2^z + \sigma_4^y \sigma_5^z \right). \quad (27)$$

If we use conjugation by U_{D_σ} to bring the defect on site 1 to site 4 we get the Hamiltonian

$$H_{D_\sigma \times D_\sigma} = - \left(\sum_{i \neq 3,4} \sigma_i^z \sigma_{i+1}^z + \sum_{i \neq 4} \sigma_i^x + \sigma_3^z \sigma_4^x \sigma_5^z \right) \quad (28)$$

This is like the usual Ising Hamiltonian of $n-1$ spins but now with an extra spin (the 4th one) that is otherwise decoupled, but controls the coupling between spins 3 and

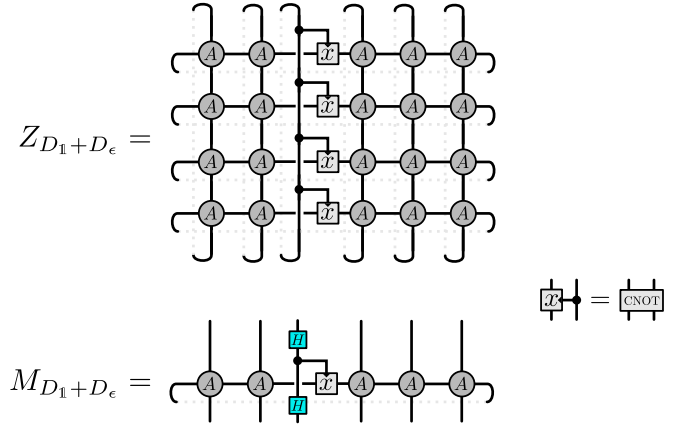


Figure 14. The partition function $Z_{D_1 + D_\epsilon}$ and its transfer matrix $M_{D_1 + D_\epsilon}$ that is the classical equivalent of $H_{D_\sigma \times D_\sigma}$. CNOT is a controlled-NOT gate $|0\rangle\langle 0| \otimes \mathbb{1} + |1\rangle\langle 1| \otimes \sigma^x$ with the dot marking the control qubit. $H = \frac{1}{2}(\sigma^x + \sigma^z)$ is the Hadamard matrix that transforms between the spin basis and the parity eigenbasis. Because $H^2 = \mathbb{1}$ the presence of the Hadamards in the transfer matrix does not affect the partition function but it ensures the transfer matrix is spin-flip invariant.

5. $H_{D_\sigma \times D_\sigma}$ is invariant under $\sigma_4^x H_{D_\sigma \times D_\sigma} \sigma_4^x$ and we can decompose it into two sectors according to the parity of the 4th spin. In the $+1$ sector the coupling between spins 3 and 5 is ferromagnetic and we have the usual Ising chain of $n-1$ spins. In the parity -1 sector the coupling is antiferromagnetic and we get the Hamiltonian for the Ising model with D_ϵ defect. This is the sense in which $D_\sigma \times D_\sigma = D_1 + D_\epsilon$ in the quantum Ising model.

B. Tensor network representation

Since we do not know how to represent the duality defect D_σ in the classical Ising model, a priori we also do not know how to insert it into a tensor network $Z_{n,m}(A)$ [see Fig. 3(a)]. However, because of the duality between the classical transfer matrix and the quantum Hamiltonian, one would expect that if we had a transfer matrix M_{D_σ} with a D_σ line defect looping through it, conjugating M_{D_σ} with the unitary U_{D_σ} would move the defect. We can make use of this intuition and the fusion rule $D_\sigma \times D_\sigma = D_1 + D_\epsilon$ to construct a tensor for D_σ . As a reminder, in Fig. 15(a) we have written the operator U_{D_σ} using the tensor network notation. In the quantum Hamiltonian $H_{D_\sigma \times D_\sigma}$, having two duality defects D_σ on site k appeared as the term $\sigma_{k-1}^z \sigma_k^x \sigma_{k+1}^z$. The tensor network analog of this is an auxiliary spin in the network that, when written in the parity eigenbasis, controls the coupling along a defect line. The partition function $Z_{D_1 + D_\epsilon}$ and the transfer matrix $M_{D_1 + D_\epsilon}$ that implement such defect are shown in Fig. 14.

We now have a tensor representing two duality defects D_σ on the same site: the CNOT with the two Hadamard gates. We can move one of the defects away by conjugating with U_{D_σ} , thus obtaining the tensor for a single

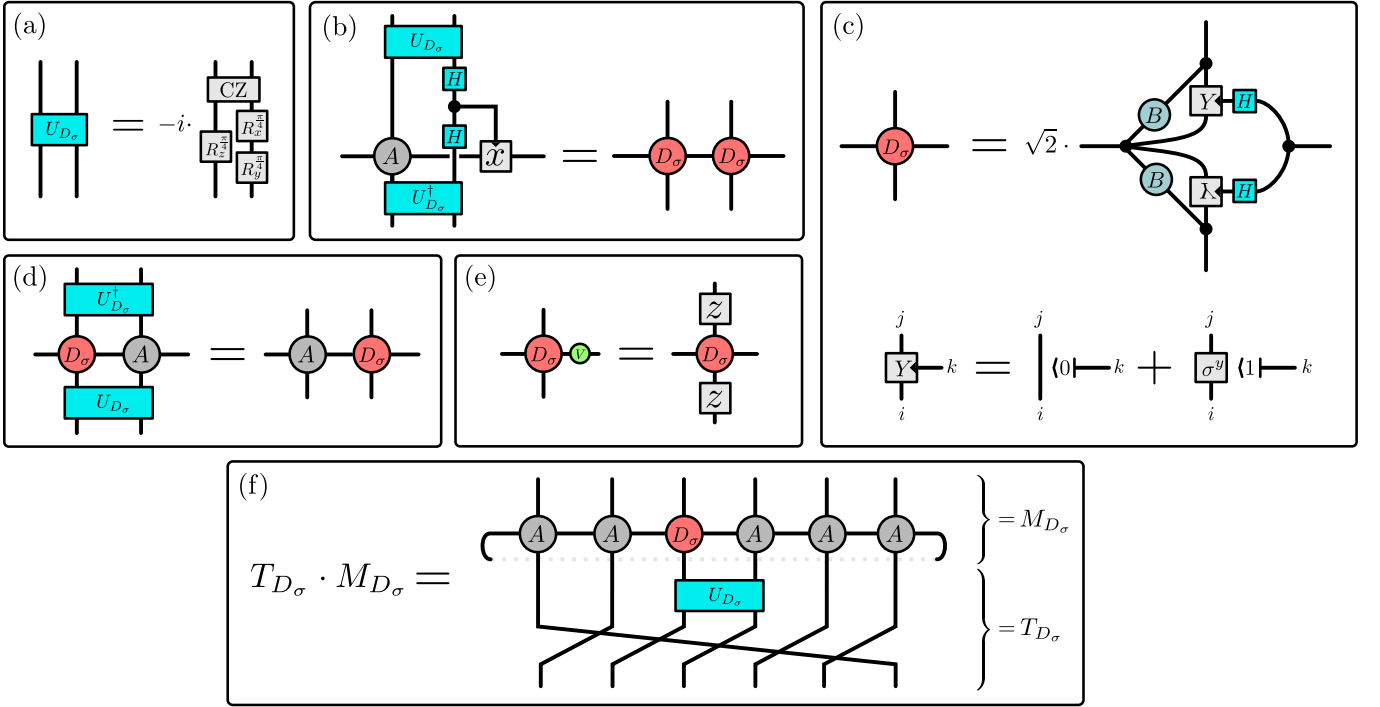


Figure 15. (a) The unitary that moves the D_σ defect by one site. Here $R_\alpha^\sigma = e^{i\alpha\sigma^\alpha} = \mathbb{1} \cos(\alpha) + i\sigma^\alpha \sin(\alpha)$ with σ^α 's being the Pauli matrices. CZ denotes a controlled-Z gate $|0\rangle\langle 0| \otimes \mathbb{1} + |1\rangle\langle 1| \otimes \sigma^z$. Compared to the U_{D_σ} in Eq. (24) this one has an additional factor of $-i$. We are in fact free to multiply U_{D_σ} with an arbitrary phase, because to move a defect we multiply it with U_{D_σ} and $U_{D_\sigma}^\dagger$ and the phases cancel. Because of this phase freedom in U_{D_σ} , when extracting the conformal spins from the eigenvalues of the translation operator [see Eq. (12)] the conformal spins are only determined up to an additive constant. The phase has been chosen here so that the conformal spins come out correctly, which relies on us knowing at least one of the exact conformal spins of the operators in Z_{D_σ} . (b) Taking the tensor network equivalent of having two D_σ defects on the same site and moving one of them away with U_{D_σ} yields two copies of the same tensor contracted with each other. We call this tensor D_σ and identify it as the tensor representing a single duality defect. Its explicit form is shown in (c). (c) The D_σ tensor obtained using the procedure in (b). $B_{ij} = e^{\beta\sigma_i\sigma_j}$ are the Boltzmann weights of the Ising model, H is the Hadamard operator $H = \frac{1}{\sqrt{2}}(\sigma^z + \sigma^x)$, and the dots are Kronecker δ 's that fix all their indices to have the same value. Note how the tensor marked with a Y , defined at the bottom as $\mathbb{1} \otimes |0\rangle\langle 0| + \sigma^y \otimes |1\rangle\langle 1|$, is almost like a controlled-Y gate. λ denotes the same tensor but with the indices i and j transposed. (d) The D_σ defect as represented by the tensor in (c) can be unitarily moved by conjugating with U_{D_σ} . (e) The fusion rule $D_\sigma \times D_\epsilon = D_\sigma$ as it manifests in the defect tensors. z denotes the σ^z Pauli matrix. (f) M_{D_σ} composed with the translation operator T_{D_σ} that commutes with it.

D_σ defect, as shown in Fig. 15(b). The explicit form of the tensor we obtain is shown in Fig. 15(c). We have omitted the calculation deriving this form as it is a long and uninformative exercise in using the properties of Pauli matrices.

The form of the D_σ tensor shown in Fig. 15(c) is physically intuitive though: The Kramers-Wannier duality maps the Ising model to an equivalent model on the dual lattice (with a degree of freedom in every plaquette). Recall how the D_ϵ defect can be seen as separating two parts of the system, one of which has been transformed with a spin-flip and the other one has not. Similarly the D_σ defect is the boundary separating a part of the system that has been mapped with the Kramers-Wannier duality from the part that has not. At this boundary we would expect spins on the dual lattice side [in Fig. 15(c) on the right] to represent domain walls between spins of the original lattice [left, top and bottom in Fig. 15(c)]. The

tensor $Y_{ijk} = \mathbb{1}_{ij} \delta_{0,k} + \sigma_{ij}^y \delta_{1,k}$ does exactly that: $Y_{ijk} \neq 0$ if and only if $k = 0$ and $i = j$ (no domain wall between spins i and j) or $k = 1$ and $i \neq j$ (a domain wall between spins i and j). The index k of Y_{ijk} (marked in the figure with a small arrowhead) thus directly represents a domain wall and it is related to the free index on the right by a simple Hadamard rotation. The B matrices meanwhile provide the usual Ising couplings between the spins of the original lattice.

The tensor for the duality defect D_σ fulfills the property that it moves by one lattice site under conjugation by U_{D_σ} , as illustrated in Fig. 15(d). We can also observe the fusion rule $D_\sigma \times D_\epsilon = D_\sigma$ by multiplying the D_σ tensor with V as in Fig. 15(e). The result is the same tensor D_σ multiplied by two Pauli matrices σ^z from above and below. This represents the same defect, because the Pauli matrices only provide a local change of basis.

Thus we propose the transfer matrix M_{D_σ} for the

twisted partition function Z_{D_σ} to be the one in Fig. 15(f). The validity of this choice is ultimately confirmed by the numerical results shown below. As with the symmetry defect D_ϵ , the usual lattice translation T moves the duality defect D_σ and we need to build a generalized translation operator $T_{D_\sigma} = U_{D_\sigma} T$ that commutes with M_{D_σ} . This, too, is shown in Fig. 15(f).

In Fig. 16, we show scaling dimensions and conformal spins $\{\Delta_\alpha, s_\alpha\}_{D_\sigma}$ for the operators in Z_{D_σ} , obtained by diagonalizing $T_{D_\sigma} \cdot M_{D_\sigma}$ for 18 sites. The results reproduce the expected conformal towers, confirming that our choice of tensor D_σ indeed represents the duality defect. Again, the accuracy of the numerical estimates quickly deteriorates with increasing scaling dimensions. Next, we will discuss how to coarse-grain in the presence of a D_σ defect, which will let us reach larger system sizes and more accurate results.

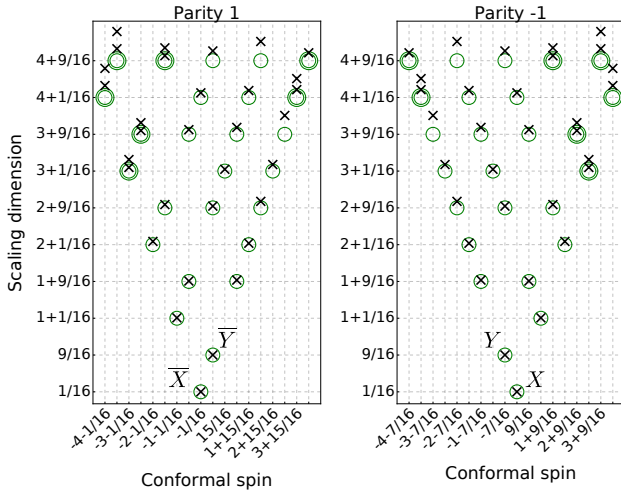


Figure 16. The scaling dimensions (vertical axis) and conformal spins (horizontal axis) of the first scaling operators in Z_{D_σ} obtained from exact diagonalization of a transfer matrix of $n = 18$ sites. The scaling operators are again divided by their \mathbb{Z}_2 charge. The crosses mark the numerical values that can be compared with the circles that are centered at the exact values. Several concentric circles denote the degeneracy N_α of that $(\Delta_\alpha, s_\alpha)$ pair.

C. Coarse-graining

Coarse-graining the symmetry defect D_ϵ was particularly simple because the global \mathbb{Z}_2 symmetry is explicitly realized in the individual tensors of the tensor network. This is no longer the case for the Kramers-Wannier self-duality. As a result, we need to coarse-grain the tensors for D_σ as we would coarse-grain any other line of impurity tensors (representing a generic conformal defect), that is, without being able to exploit that they correspond to a topological defect. For a sufficiently local coarse-graining scheme, such as TNR¹⁸ (but also TRG²⁰ and its gener-

alizations, see Sec. VIII), a line defect is coarse-grained into a line defect at the next scale. The details of how we coarse-grain the line defect using TNR are explained in Appendix A. The same appendix also shows how the translation operator T_{D_σ} is coarse-grained in this process.

Under TNR, the duality defect D_σ is coarse-grained into a line defect with a width of two tensors. The coarse-grained transfer matrix $M_{D_\sigma}^{(s)}$ and translation operator $T_{D_\sigma}^{(s)}$ are thus as shown in Fig. 17. The operator $T_{D_\sigma}^{(s)} \cdot M_{D_\sigma}^{(s)}$ can then be exactly diagonalized and its eigenvalue spectrum yields the scaling dimensions and conformal spins $\{\Delta_\alpha, s_\alpha\}_{D_\sigma}$ of the scaling operators with lowest dimensions in Z_{D_σ} . There is, however, a small technical subtlety in how to extract the conformal data from the spectrum that is discussed in Appendix D.

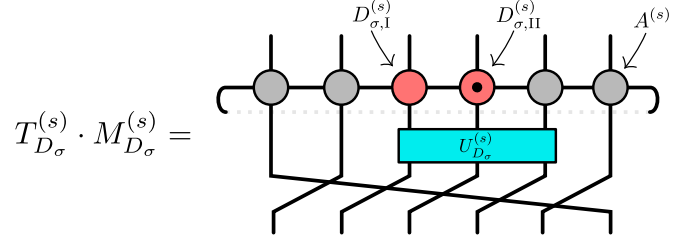


Figure 17. The coarse-grained transfer matrix for the D_σ defect composed with the generalized translation $T_{D_\sigma}^{(s)}$.

D. Numerical results

As discussed earlier, the primaries present in Z_{D_σ} are the ones with the conformal dimensions $(\frac{1}{2}, \frac{1}{16})$, $(0, \frac{1}{16})$, $(\frac{1}{16}, \frac{1}{2})$ and $(\frac{1}{16}, 0)$. The first two have parity +1, the latter two -1. Numerical results for the scaling dimensions and conformal spins of these primaries obtained with the TNR method are shown in Table IV. Similar values for some of the first descendants are shown in Fig. 18. The results are again in excellent agreement with the exact results even higher up in the conformal towers. These results were obtained by coarse-graining a transfer matrix of $2^5 \times (4 \times 2^5)$ $A^{(0)}$ tensors using TNR with bond dimensions $\chi = 22$ and $\chi' = 11$. Again, a slightly larger system was used for obtaining the conformal spins, see Appendix B.

E. MERA

As was the case with the D_1 and D_ϵ defects, coarse-graining the network for Z_{D_σ} with TNR produces a MERA for the ground state of the spin chain with D_σ defect. This MERA is shown in Fig. 19. As the figure shows, only the tensors within the causal cone of the defect are different from the ones in the D_1 MERA in Fig. 8. Such a MERA is known as an impurity MERA²⁷. It should be noted that unlike for a general impurity MERA the

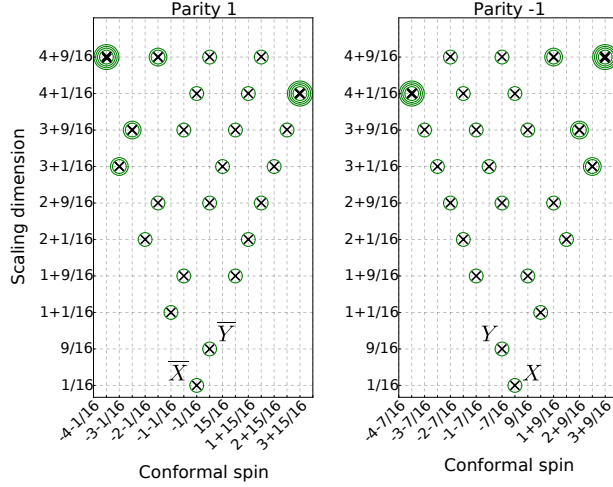


Figure 18. The scaling dimensions (vertical axis) and conformal spins (horizontal axis) of the first scaling operators of the two-dimensional classical Ising model with a D_σ defect as obtained with TNR. The crosses mark the numerical values that can be compared with the circles that are centered at the exact values. Several concentric circles denote the degeneracy N_α of that $(\Delta_\alpha, s_\alpha)$ pair. The keen-eyed reader may notice that high up in the conformal towers some of the momenta differ from those shown in Fig. 16. This is because the periodicity of the momenta in these results is lower, so that for instance the conformal spins $-4 + \frac{7}{16}$ and $4 + \frac{7}{16}$ are indistinguishable.

Primary	(h, \bar{h})	Δ_{TNR}	Δ_{exact}	s_{TNR}	s_{exact}
X	$(1/16, 0)$	0.0626656	0.0625	0.0624974	0.0625
\bar{X}	$(0, 1/16)$	0.0626656	0.0625	-0.0624974	-0.0625
Y	$(1/16, 1/2)$	0.5627685	0.5625	-0.4374828	-0.4375
\bar{Y}	$(1/2, 1/16)$	0.5627685	0.5625	0.4374828	0.4375

Table IV. The scaling dimensions Δ and conformal spins s for the primaries of Z_{D_σ} as obtained with TNR compared with the exact values. Note that, as with D_ϵ , one can analytically deduce the possible values of the conformal spins in the two parity sectors by observing that $(T_{D_\sigma})^{2n-1} = \frac{1}{\sqrt{2}}(\mathbb{1} + i\Sigma^x)$, where Σ^x is the global spin-flip operator. However, we choose to present the numerical values for the conformal spins, including the small numerical errors, to demonstrate the accuracy of our method.

impurity tensors in Fig. 19 can be moved with the unitary operator U_{D_σ} .

VII. GENERIC CONFORMAL DEFECTS

This paper is devoted to the study of topological conformal defects using tensor network techniques. As discussed in the introduction, the main difference between a generic (i.e. non-topological) conformal defect and a topological conformal defect is that in the latter case there is a local unitary transformation that moves the location of the defect. This allowed us to define a generalized translation

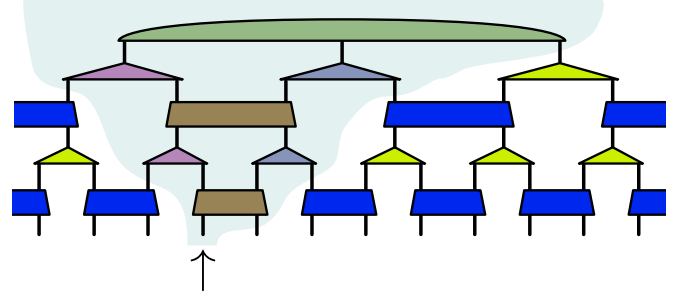


Figure 19. A MERA for the ground state of the quantum spin chain that has a duality defect in it, produced by coarse-graining Z_{D_σ} with TNR. The tensors in this MERA are the same ones that are used in coarse-graining the D_σ defect in Fig. 27. Even though our notation does not reflect it, the unitaries and isometries on different layers generally differ from each other. The arrow marks the position of the defect and the pale blue region is the causal cone of the defect site.

operator T_D whose eigenvalues yield the conformal spins s_α associated with the defect D .

For a non-topological defect, the absence of a local unitary transformation that moves the defect implies that we can no longer define the translation operator T_D , and therefore we cannot extract conformal spins. However, we can still build a tensor network representation of a non-topological defect D , and thus of the corresponding partition function Z_D on a torus and its transfer matrix M_D . In addition, we can still coarse-grain and diagonalize the transfer matrix M_D corresponding to a number n of sites much larger than what is accessible with exact diagonalization. The spectrum of M_D for a non-topological defect is no longer given by Eq. (10), but it still provides information about the universal properties of the system.

A. Family of defects for the Ising model

As a simple example, we consider a continuous family of conformal defects D_γ of the critical Ising model^{1,4} where the coupling between spins across the defect is proportional to a real number $\gamma \in [0, 1]$. The choice $\gamma = 0$ corresponds to no coupling across the line and thus to open boundary conditions, whereas $\gamma = 1$ corresponds to periodic boundary conditions, and thus no defect. Ignoring again finite-size corrections of higher order in n^{-1} , the eigenvalues $\lambda_\alpha(\gamma)$ of M_{D_γ} can be expressed as

$$\frac{\lambda_\alpha(\gamma)}{\lambda_0(\gamma)} = e^{-\frac{2\pi}{n} \Delta_\alpha(\gamma)}. \quad (29)$$

At $\gamma = 1$, Δ_α are the scaling dimensions of the Ising CFT. For general γ , Δ_α can be predicted analytically using a description in terms of fermionic operators. This will be discussed in detail in future work (Ref. 29). The result is that Δ_α behave linearly in $\theta = \tan^{-1} \left(\frac{1-\gamma}{1+\gamma} \right)$.

B. Numerical results

Figure 20 shows estimates for Δ_α as functions of θ , obtained by diagonalizing M_{D_γ} for a system of size $n = 18$, using exact diagonalization. The results are compared with the analytic values, which appear as lines. Figure 21 shows similar estimates obtained by diagonalizing a coarse-grained transfer matrix $M_{D_\gamma}^{(s)}$, effectively reaching a system size of roughly 4000 spins. Here we have used the same coarse-graining strategy as for the duality defect D_σ in Sec. VI, with bond dimension $\chi = 22$ and $\chi' = 11$. Again, the results obtained using coarse-graining show greater accuracy with respect to the analytic predictions, but even exact diagonalization gets many of the qualitative features of the spectrum correct.

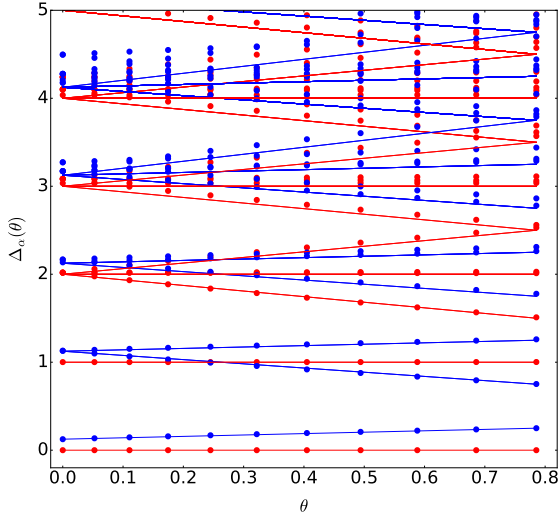


Figure 20. Numerical estimates for $\Delta_\alpha(\theta) = -\frac{n}{2\pi} \log \left(\frac{\lambda_\alpha(\theta)}{\lambda_0(\theta)} \right)$ obtained using exact diagonalization on a system of size $n = 18$. Here $\lambda_\alpha(\theta)$ are the eigenvalues of M_{D_γ} and $\theta = \tan^{-1} \left(\frac{1-\gamma}{1+\gamma} \right)$. The lines are the analytic predictions coming from free fermion calculations²⁹. The blue and red colors mark the parity odd and parity even sectors, respectively. At the extreme left at $\theta = 0$ is the case of periodic boundary conditions, where the Δ_α are the scaling dimensions of the Ising CFT. At the extreme right at $\theta = \frac{\pi}{4}$ is the case of open boundary conditions. The numerical results clearly show qualitative agreement with the analytic values, but accuracy deteriorates significantly after the first few Δ_α 's.

VIII. DISCUSSION

In this paper, we have explained how to compute accurate numerical estimates of the scaling dimensions and conformal spins $\{\Delta_\alpha, s_\alpha\}_D$ associated to a topological conformal defect D , or the scaling dimensions $\{\Delta_\alpha\}_D$ associated to a generic (i.e., non-topological) conformal

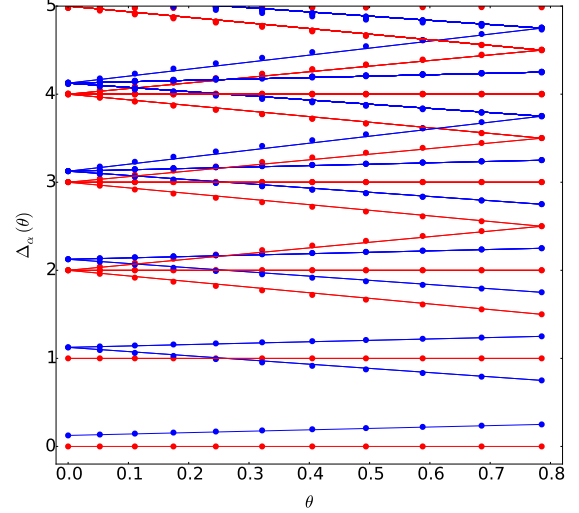


Figure 21. Numerical estimates for $\Delta_\alpha(\theta) = -\frac{n}{2\pi} \log \left(\frac{\lambda_\alpha(\theta)}{\lambda_0(\theta)} \right)$ obtained by coarse-graining and then diagonalizing a transfer matrix for a system of roughly 4000 spins. $\lambda_\alpha(\theta)$ are the eigenvalues of M_{D_γ} and $\theta = \tan^{-1} \left(\frac{1-\gamma}{1+\gamma} \right)$. As in Fig. 20, $\theta = 0$ corresponds to periodic boundary conditions, $\theta = \frac{\pi}{4}$ corresponds to open boundary conditions and the lines are the analytic predictions coming from free fermion calculations²⁹. The blue and red colors mark the parity odd and parity even sectors, respectively. The numerical and analytic values are seen to agree to a high precision, owing to the fact that the coarse-graining has significantly reduced finite-size effects.

defect D . For simplicity, we have focused on the topological conformal defects of the critical Ising model, namely the symmetry defect D_ϵ and duality defect D_σ , and have briefly considered also a family of non-topological, conformal defects. In order to improve significantly on the numerical estimates readily available through exact diagonalization, we have used a particular coarse-graining transformation: tensor network renormalization (TNR). Our numerical results clearly demonstrated that tensor network techniques are a useful tool to characterize conformal defects in critical lattice models.

We conclude this paper with a short discussion on applying this approach to other lattice models, on using other coarse-graining schemes for the same purpose, and on an alternative, more direct route to extracting conformal data from critical lattice models based on building a lattice version of the scaling operators of the theory.

A. Conformal defects in other models

The tensor network approach described in this paper can be applied to line defects on any critical 2D classical partition function on the lattice (or point defects on any critical 1D quantum lattice system). Let us recall what the requirements of the approach are.

The scaling dimensions $\{\Delta_\alpha\}_D$ associated to a conformal defect D can be extracted from the eigenvalues of the transfer matrix M_D for the partition function Z_D that includes that defect. Thus, we only need to have a lattice representation of the line defect D , from which to build Z_D and M_D .

In addition, for a topological conformal defect D , the associated conformal spins $\{s_\alpha\}_D$ can be extracted from the eigenvalues of a generalized translation operator T_D , built by composing a one-site translation with the application of the local unitary transformation that moves the defect back to its initial position, as explained in Secs. V and VI for the symmetry defect D_ϵ and duality defect D_σ of the critical Ising model. Thus, in this case we also need to have a lattice representation of the local unitary transformation that moves the location of the defect D .

Symmetry defects, associated to a global internal symmetry group \mathcal{G} , are a type of topological conformal defect that is particularly easy to deal with within the tensor network formalism. Indeed, as we did in the case of the \mathbb{Z}_2 group of the Ising model, for each group element $g \in \mathcal{G}$ we can create a line defect D_g as a form of twisted boundary conditions by inserting copies of a unitary representation V_g along a vertical line of bond indices. This is remarkably simple when using \mathcal{G} -symmetric tensors to represent the tensor network. In this case, each tensor index is labeled by irreducible representations of \mathcal{G} , and V_g acts diagonally on the irreducible representations by placing a different complex phase on each of the them. As in the Ising model, the position of the line defect can be moved by a local unitary transformation that acts on single sites. Thus, we have all the required elements to extract both scaling dimensions and conformal spins for any defect arising from an internal symmetry. This is illustrated in Appendix C by presenting results for the symmetry defects of the 3-state Potts model.

Duality defects are in general more difficult to characterize, but a lattice representation is known in several models (see Ref. 28). Finding a unitary transformation that moves the duality defect ought to also be possible after a case-by-case analysis. Then, we would be able to use the tools described in this paper.

B. Why tensor network renormalization?

In this paper, we have employed a particular choice of coarse-graining transformation, namely, the tensor network renormalization (TNR) scheme, to coarse-grain the tensor network representation of the generalized transfer matrix M_D and translation operator T_D corresponding to a topological defect D , in order to extract accurate estimates of the associated scaling dimensions and conformal spins $\{\Delta_\alpha, s_\alpha\}_D$ (or just $\{\Delta_\alpha\}_D$ for a generic conformal defect). However, we could have used many other coarse-graining schemes.

Indeed, any coarse-graining transformation that accurately preserves the spectra of M_D and T_D will allow

us to extract the conformal data. Examples of such coarse-graining transformations include tensor renormalization group (TRG)²⁰, higher-order tensor renormalization group (HOTRG)³⁰, tensor entanglement-filtering renormalization (TEFR)⁷, the second renormalization group (SRG)³¹, and higher-order second renormalization group (HOSRG)³⁰.

TRG is the simplest option, and already produces a very significant gain of accuracy with respect to exact diagonalization, since much larger systems can be considered for an equivalent computational cost, without introducing significant truncation errors, so that the estimates for $\{\Delta_\alpha, s_\alpha\}_D$ are less affected by non-universal, finite-size corrections.

The accuracy of TRG can be further increased, for the same bond dimension and similar computational cost, in a number of ways. Several improved algorithms, such as SRG and HOSRG, are based on computing an environment that accounts for the rest of the tensor network during the truncation step of the coarse-graining. The use of a global environment has the important advantage that it leads to a better truncation of bond indices, and thus to more accurate results, compared to an equivalent scheme that does not employ the environment (for instance, SRG compared to TRG, or HOSRG compared to HOTRG).

However, in the context of studying defects, the use of a global environment also has a second, less favorable implication. Since in order to truncate a given bond index we use a cost function that is aware of the whole tensor network, the resulting coarse-grained tensors will notice the presence of the defect even when the defect is away from those tensors (recall that in a critical systems correlations decay as a power-law with the distance). Consider a tensor network for the partition function Z_D with line defect D , where the line defect is initially characterized by a column of tensors that is inserted into the tensor network for the partition function Z in the absence of the defect, as we have done in this work. Then under a coarse-graining transformation such as SRG or HOSRG, the coarse-grained tensor network will consist of a collection of different tensors that depend on their distance to the defect. In other words, the representation of the defect will spread throughout the whole tensor network, instead of remaining contained in a (single or double) column of tensors, as was the case in this paper. As a matter of fact, for topological defects this can be prevented through a careful analysis, since in some sense these defects can be made invisible to neighboring tensors (since their location can be changed through local unitary transformations). For generic conformal defects, however, one needs to consider a mixed strategy where the global environment is used in order to coarse-grain the partition function Z in the absence of a defect, as well as the defect tensors in Z_D , but is not used in order to coarse-grain the rest of tensors in Z_D , which are recycled from Z .

A direct comparison of computational resources required by several of these approaches has shown that TNR provides significantly more accurate estimates than

the above methods for $\{\Delta_\alpha, s_\alpha\}$ from the transfer matrix M and translation operator T in the absence of a defect, see e.g. Ref. 18. The ultimate reason is that TNR, thanks to the use of disentanglers to remove short-range correlations/entanglement in the partition function, provides a much more accurate description of the partition function when using tensors with the same bond dimension. We expect the same to be true for the estimation of $\{\Delta_\alpha, s_\alpha\}_D$ from the transfer matrix M_D and translation operator T_D in the presence of a topological defect D (or just $\{\Delta_\alpha\}_D$ from M_D in the presence of a generic conformal defect D).

It is worth emphasizing, however, that a simpler algorithm such as TRG, which is easier to code, already provides much better accuracy than exact diagonalization.

C. Alternative approach to extracting conformal data from a critical lattice model

In this paper, we have extracted the scaling dimensions and conformal spins $\{\Delta_\alpha, s_\alpha\}_D$ associated to a topological conformal defect D by diagonalizing the transfer matrix M_D and translation operator T_D of a corresponding partition function Z_D on the lattice. This approach is based on generalizing, to the case of a line defect, the observation of Ref. 7 that the operator-state correspondence of a CFT allows us to extract the scaling dimensions and conformal spins $\{\Delta_\alpha, s_\alpha\}$ of local scaling operators of the underlying CFT by diagonalizing the transfer matrix M and translation operator T of the clean partition function Z_D on the lattice. Indeed, as discussed in Sec. II, the operator-state correspondence relates the scaling operators ϕ_α of the theory with the energy and momentum eigenvectors $|\alpha\rangle$ of the Hamiltonian H and momentum P operators of the same theory (where the transfer matrix M and the translation operator T can be thought of as the exponentials of H and P , respectively), allowing the extraction of $\{\Delta_\alpha, s_\alpha\}$ directly from (a properly normalized version of) the spectra of energies and momenta $\{E_\alpha, p_\alpha\}$.

An alternative, more direct way of extracting $\{\Delta_\alpha, s_\alpha\}$ from a lattice system is also possible, by identifying a lattice version of the corresponding scaling operators ϕ_α , and studying their transformation properties under changes of scale and rotations. This alternative approach was recently made possible by the introduction of the tensor network renormalization (TNR)^{18,32}. The key of the approach is that, through the use of disentanglers that eliminate short-range correlations / entanglement from the coarse-grained partition function Z , at criticality it is possible to explicitly realize scale invariance: the tensor network before and after coarse-graining is expressed in terms of the same critical fixed-point tensor. As explained in Ref. 32, it is then possible to build a transfer matrix R *in scale*, representing a lattice version of the dilation operator of the CFT, whose eigenvectors correspond to

a lattice version of the scaling operators ϕ_α , while the eigenvalues are the exponential of the scaling dimensions Δ_α (conformal spins s_α are also extracted by analysis of two-point correlators).

This direct approach is computationally more challenging, since it requires ensuring that scale invariance is explicitly realized during the coarse-graining, before building and diagonalizing the scale transfer matrix R . However, it also has some remarkable advantages. On the one hand, it appears to provide even more accurate results for $\{\Delta_\alpha, s_\alpha\}$ than the diagonalization of the space-time transfer matrix M discussed in this paper, see Appendix in Ref. 32. Even more important is the fact that, using the explicit lattice representation of the scaling operators ϕ_α obtained from the scale transfer matrix R , we can study the fusion of two such operators into a third one, thus yielding the operator product expansion (OPE) coefficients of the CFT, which can not be obtained from the space-time transfer matrix M . These possibilities extend to the presence of defects, as demonstrated in Ref. 32 for the symmetry defect D_ϵ of the Ising model.

Finally, we also emphasize that in the context of quantum spin systems, conformal defects have already been studied using MERA. In that case, scale invariance was explicitly used to extract the scaling dimensions Δ_α attached to a conformal defect that represented an impurity, an open boundary or an interface between two critical systems, see Refs. 33 and 27.

Note added. A few weeks after this manuscript was posted on the arXiv, Aasen, Mong, and Fendley posted a paper with independent, closely related work on topological defects of the classical square-lattice Ising model³⁴. While the emphasis in our paper is on the use of tensor network methods, Ref. 34 is centered on constructing analytical models. Thus, the two papers nicely complement each other.

We thank our anonymous referees for valuable feedback. M. Hauru thanks Andrew Tinitis for helpful discussions on the numerical aspects of this work. M. Hauru is supported by an Ontario Trillium Scholarship. G. Vidal and G. Evenbly acknowledge support by the Simons Foundation (Many Electron Collaboration). G. Vidal also acknowledges support by the John Templeton Foundation. The authors also acknowledge support by Calcul Québec and Compute Canada. This research was supported in part by Perimeter Institute for Theoretical Physics. Research at Perimeter Institute is supported by the Government of Canada through the Department of Innovation, Science and Economic Development Canada and by the Province of Ontario through the Ministry of Research, Innovation and Science.

-
- * markus@mhauru.org
- ¹ M. Oshikawa and I. Affleck, Nuclear Physics B **495**, 533 (1997), arXiv:cond-mat/9612187.
 - ² P. di Francesco, P. Mathieu, and D. Sénéchal, *Conformal Field Theory*, Graduate Texts in Contemporary Physics (Springer, New York, 1997).
 - ³ M. Henkel, *Conformal Invariance and Critical Phenomena* (Springer, Berlin, Heidelberg, 1999).
 - ⁴ I. Affleck, arXiv:0809.3474 (2008).
 - ⁵ T. Quella, I. Runkel, and G. M. T. Watts, Journal of High Energy Physics **2007**, 095 (2007), arXiv:hep-th/0611296.
 - ⁶ V. B. Petkova and J.-B. Zuber, Physics Letters B **504**, 157 (2001), arXiv:hep-th/0011021.
 - ⁷ Z.-C. Gu and X.-G. Wen, Physical Review B **80**, 155131 (2009), arXiv:0903.1069.
 - ⁸ S. Singh, R. N. C. Pfeifer, and G. Vidal, Physical Review B **83**, 115125 (2011), arXiv:1008.4774.
 - ⁹ R. J. Baxter, *Exactly Solved Models in Statistical Mechanics* (Academic Press, London, 1982).
 - ¹⁰ U. Grimm and G. M. Schuetz, Journal of Statistical Physics **71**, 923 (1993), arXiv:hep-th/0111083.
 - ¹¹ S. Sachdev, *Quantum phase transitions* (Cambridge University Press, Cambridge; New York, 2011).
 - ¹² P. Ginsparg, arXiv:hep-th/9108028 (1988).
 - ¹³ J. L. Cardy, Nuclear Physics B **270**, 186 (1986).
 - ¹⁴ In a finite system M only has a finite number of eigenvalues whereas there is an infinite number of scaling operators. However, we do observe that at least the largest λ_α 's correspond to the scaling operators with smallest Δ_α , see Fig. 2.
 - ¹⁵ R. Orus and G. Vidal, Physical Review B **78**, 155117 (2008), arXiv:0711.3960.
 - ¹⁶ S. Singh, R. N. C. Pfeifer, and G. Vidal, Physical Review A **82**, 050301 (2010), arXiv:0907.2994.
 - ¹⁷ S. Singh and G. Vidal, Physical Review B **86**, 195114 (2012), arXiv:1208.3919.
 - ¹⁸ G. Evenbly and G. Vidal, Physical Review Letters **115**, 180405 (2015), arXiv:1412.0732.
 - ¹⁹ G. Evenbly, arXiv:1509.07484 (2015).
 - ²⁰ M. Levin and C. P. Nave, Physical Review Letters **99**, 120601 (2007), arXiv:cond-mat/0611687.
 - ²¹ G. Evenbly and G. Vidal, Physical Review Letters **115**, 200401 (2015), arXiv:1502.05385.
 - ²² We have dropped here the previous distinction between the partition function Z of a lattice model and Z_{CFT} of the CFT: Here by Z_D we mean a field theory partition function, whereas later we will use the same symbol to refer to its lattice realization. Context should make clear which one we are referring to.
 - ²³ J. Fröhlich, J. Fuchs, I. Runkel, and C. Schweigert, Nuclear Physics B **763**, 354 (2007), arXiv:hep-th/0607247.
 - ²⁴ J. Fröhlich, J. Fuchs, I. Runkel, and C. Schweigert, Physical Review Letters **93**, 070601 (2004), arXiv:cond-mat/0404051.
 - ²⁵ G. von Gehlen and V. Rittenberg, Journal of Physics A: Mathematical and General **20**, 227 (1987).
 - ²⁶ P. Chaselon, Journal of Physics A: Mathematical and General **22**, 2495 (1989).
 - ²⁷ G. Evenbly and G. Vidal, Journal of Statistical Physics **157**, 931 (2014), arXiv:1312.0303.
 - ²⁸ C. H. O. Chui, C. Mercat, W. Orrick, and P. A. Pearce, Physics Letters B **517**, 429 (2001), arXiv:hep-th/0106182.
 - ²⁹ M. Hauru, D. Gaiotto, G. Vidal, *et al.*, In preparation.
 - ³⁰ Z. Y. Xie, J. Chen, M. P. Qin, J. W. Zhu, L. P. Yang, and T. Xiang, Physical Review B **86**, 045139 (2012), arXiv:1201.1144.
 - ³¹ Z. Y. Xie, H. C. Jiang, Q. N. Chen, Z. Y. Weng, and T. Xiang, Physical Review Letters **103**, 160601 (2009), arXiv:0809.0182.
 - ³² G. Evenbly and G. Vidal, arXiv:1510.00689 (2015).
 - ³³ G. Evenbly, R. N. C. Pfeifer, V. Pico, S. Iblisdir, L. Tagliacozzo, I. P. McCulloch, and G. Vidal, Physical Review B **82**, 161107 (2010), arXiv:0912.1642.
 - ³⁴ D. Aasen, R. S. K. Mong, and P. Fendley, arXiv:1601.07185 (2016).
 - ³⁵ G. Vidal, Physical Review Letters **101**, 110501 (2008), arXiv:quant-ph/0610099.
 - ³⁶ This is related to the causal cone of the binary MERA that is two sites wide for certain operators^{21,35}.
 - ³⁷ G. Evenbly and G. Vidal, Physical Review B **79**, 144108 (2009), arXiv:0707.1454.

Appendix A: Tensor network renormalization

This appendix gives a quick overview of the tensor network renormalization (TNR) scheme that we use and shows how to adapt it to coarse-graining the topological defects D_ϵ and D_σ of the Ising model. It also shows how the translation operators T , T_{D_ϵ} and T_{D_σ} are coarse-grained in the process.

TNR is a coarse-graining transformation for tensor networks that is based on inserting approximate partitions of unity into the network and optimizing them to minimize the truncation error. It removes all short-range correlations during the coarse-graining and thus manages to realize a proper renormalization group flow with the right fixed point structure. Full details of the algorithm can be found in Refs. 18 and 19 and will not be repeated here. As a summary and a reminder, Fig. 22 shows the progression of a TNR coarse-graining step. It shows how a network $Z_{n,m}(A^{(i)})$ is coarse-grained into a new network $Z_{\frac{n}{2}, \frac{m}{2}}(A^{(i+1)})$, where each tensor $A^{(i+1)}$ corresponds to four $A^{(i)}$'s. χ and χ' mark the dimensions of the bonds. They control the accuracy of the approximations done in the algorithm but also the computational cost: Higher bond dimensions mean smaller truncation errors but require more memory and computation time.

All the tensors used in coarse-graining the Ising model are \mathbb{Z}_2 invariant in the following sense: For every bond in the network there exists a unitary matrix representation V of the non-trivial element of \mathbb{Z}_2 , called the spin-flip matrix of that bond, such that for any tensor t in the network, multiplying all the legs of t with the appropriate spin-flip matrix gives back t again. The spin-flip matrices for the different bonds are in general different, but we use V or $V^{(i)}$ to denote all of them: The bond they are on defines the correct V unambiguously. Figure 23 illustrates, as an example, the \mathbb{Z}_2 invariance of the w tensor. Information on how such symmetry properties can be implemented and how to make computational use of them can be found in Refs. 8, 16, and 17.

If we coarse-grain a transfer matrix multiplied with a lattice translation by two sites, the translation is coarse-grained into translation by one site at the next scale, as shown in Fig. 24. More generally, a translation by an even number of sites n is coarse-grained into a translation by $\frac{n}{2}$ sites at the next scale. Because of this, the translation operator $T^{(s)}$ [Fig. 6, back in Sec. III] is a translation by 2^s sites at the original scale. Thus the eigenvalues of $T^{(s)}$ are $\left(e^{\frac{2\pi i}{2^s n_s} s \alpha}\right)^{2^s} = e^{\frac{2\pi i}{n_s} s \alpha}$ and the conformal spins are determined modulo n_s . To obtain the conformal spins with more possible values we can do an additional coarse-graining step on $T^{(s)} \cdot M^{(s)}$, as explained in Appendix B.

1. Coarse-graining the D_ϵ defect

The TNR coarse-graining explained above can accommodate for a D_ϵ defect without any changes. As explained

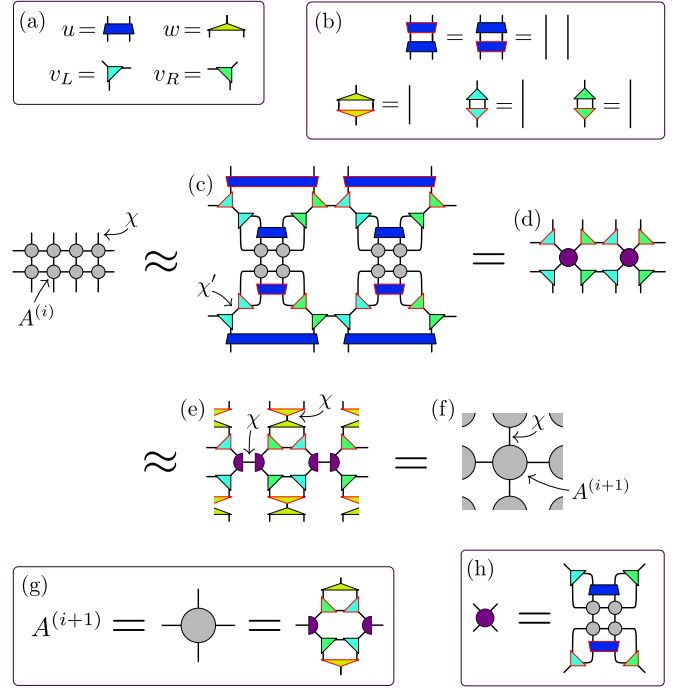


Figure 22. An overview of the tensor network renormalization procedure that we use. The network is assumed to repeat as exactly similar in all directions. χ and χ' are the (maximum allowed) dimensions of the bonds they point at and all similar bonds in the network. The tensors with red borders are complex conjugates of the ones with the same shape but with black borders. (a) The tensors used in TNR. (b) The u tensor is unitary whereas v_L , v_R and w are isometric. (c) Insertion of u 's, v_L 's and v_R 's as approximate partitions of unity. The fact that v_L and v_R are not unitary introduces a truncation error. u , v_L and v_R are optimized to minimize this error. (d) Some of the tensors have been contracted together to the one defined in (h). Because the network repeats itself in all directions the u 's and u^\dagger 's at the edges of the network have disappeared: they cancel with their counterparts in the next, similar blocks of tensors above and below the one shown. (e) Another approximate partition of unity has been inserted into the network as $w w^\dagger$ and the purple tensor has been split into two using a truncated singular value decomposition, as is done in Levin & Nave's tensor renormalization group²⁰. (f) Tensors in (e) are contracted to form the new network of tensors $A^{(i+1)}$, defined in (g).

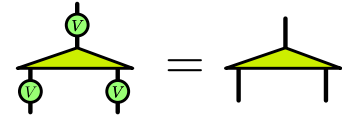


Figure 23. The \mathbb{Z}_2 invariance property of the w tensor (in yellow). V is the spin-flip matrix of the index it is on. Note that all the three V 's in this figure may in fact be different matrices, although our naming convention does not reflect this. Similar properties hold for all the tensors involved in coarse-graining the Ising model.

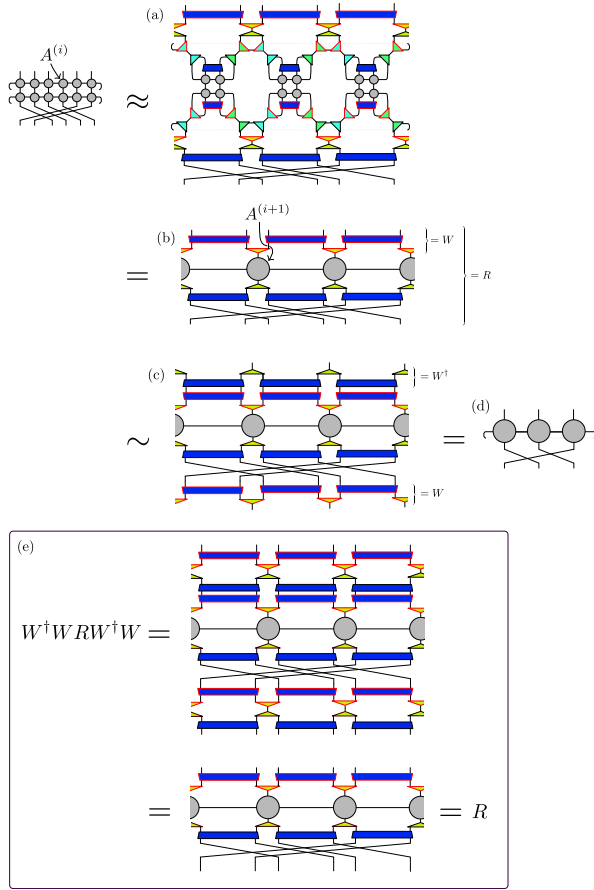


Figure 24. One step of coarse-graining for the operator $T^{(i)}$. $M^{(i)}$. The lattice translation by two sites gets coarse-grained into a translation by one site at the next scale. Periodic boundaries in the horizontal direction are assumed even when they are not explicitly shown. The tensors with red borders are complex conjugates of the ones with the same shape but with black borders. (a) The first step of the TNR algorithm has been applied to the tensors $A^{(i)}$. (b) A number of tensors are contracted to form $A^{(i+1)}$. We also define the operators W and R . (c) The operator R has been conjugated with W . \sim denotes that the operators in (b) and (c) have the spectrum, or in other words that WRW^\dagger has the same spectrum as R . This is true because, although W is isometric and not unitary, it acts like a unitary on M , as shown in (e). (d) The unitaries and isometries cancel and we are left with the coarse-grained transfer matrix and translation operator.

in Sec. V, a D_ϵ defect in a tensor network is realized by having spin-flip matrices on a string of bonds. Figure 25 shows how, using the \mathbb{Z}_2 invariance property of all the tensors in the network, such a defect coarse-grains into a similar string of spin-flip matrices at the next scale. Hence, we can coarse-grain as if there was no defect, and at any scale i we can insert a D_ϵ defect into the system as a string of spin-flip matrices $V^{(i)}$, that are the representations of the non-trivial element of \mathbb{Z}_2 under which the matrix $A^{(i)}$ is \mathbb{Z}_2 invariant.

In Sec. V, we introduced the generalized translation

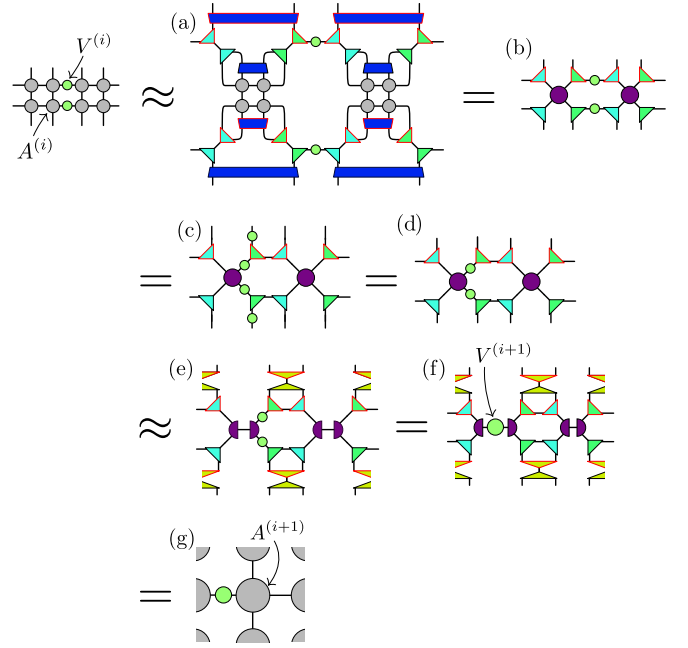


Figure 25. Coarse-graining a system with a D_ϵ defect in it. By repeatedly using the \mathbb{Z}_2 invariance of the different tensors and the fact that $(V^{(i)})^2 = \mathbb{1}$ we can take the string of spin-flip matrices $V^{(i)}$ “through” the TNR procedure to the next scale. In the figure, the network is assumed to repeat as exactly similar in all directions. The tensors with red borders are complex conjugates of the ones with the same shape but with black borders. Steps (a), (b), (e) and (g) are the same steps as taken in the usual TNR algorithm [see Fig. 22]. At steps (c) and (f) we have moved the spin-flip matrices to different legs using the \mathbb{Z}_2 invariance of the tensors and the fact that $(V^{(i)})^2 = \mathbb{1}$. At step (d) the spin-flip matrices at the top and the bottom have canceled with similar matrices coming from the parts of the network above and below the one shown here.

operator T_{D_ϵ} that is the proper notion of translation for a system with a D_ϵ defect. Figure 26 shows how the generalized two-site translation operator is coarse-grained into a generalized one-site translation at the next scale. The procedure is the same as what we did with the usual lattice translation in Fig. 24, except for the spin-flip matrices that get transferred to the next scale. Again, this generalizes to a generalized translation by an even number of sites n that is coarse-grained into a generalized translation by $\frac{n}{2}$ sites at the next scale. Thus we know how to construct the generalized translation operator $T_{D_\epsilon}^{(i)}$ at any scale with no additional numerical work needed.

2. Coarse-graining the D_σ defect

Coarse-graining the symmetry defect D_ϵ is easy because of the \mathbb{Z}_2 invariance of the tensors in the TNR procedure. The Kramers-Wannier symmetry of the critical Ising model is not similarly explicitly realized in the

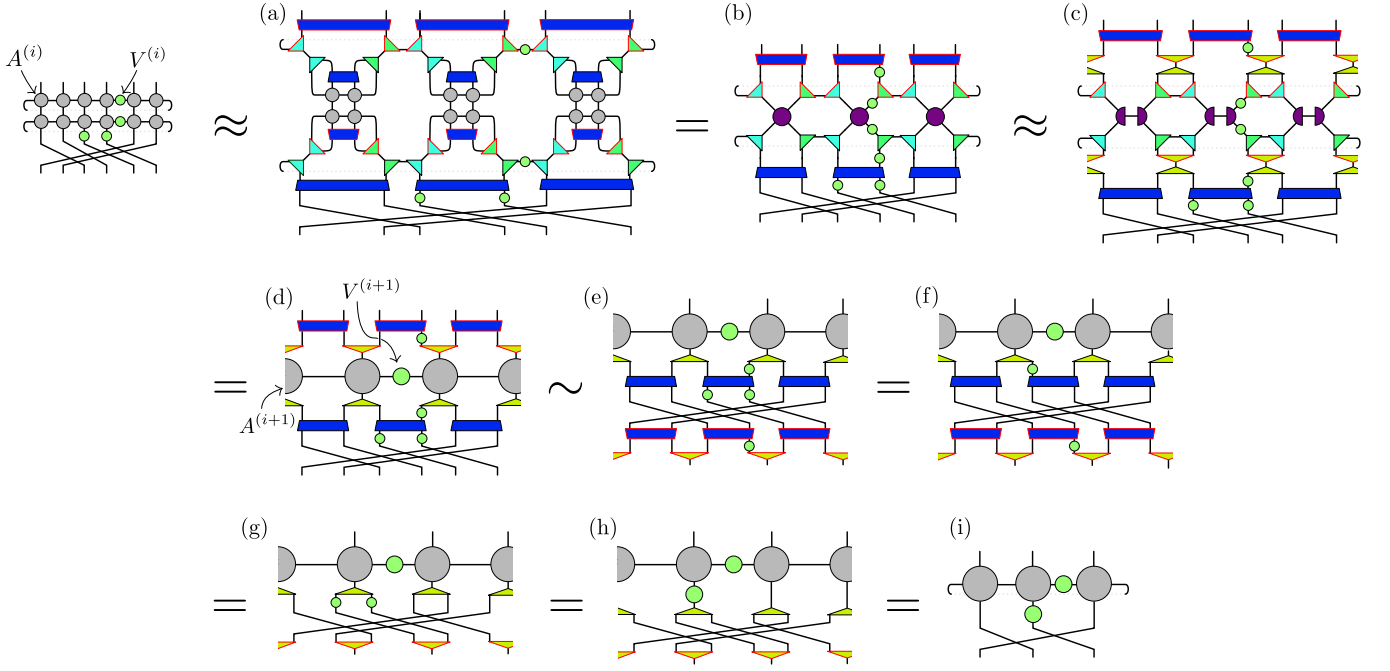


Figure 26. One step of coarse-graining for the operator $T_{D_\epsilon}^{(i)} \cdot M_{D_\epsilon}^{(i)}$. The generalized translation by two sites gets coarse-grained into a generalized translation by one site at the next scale. Periodic boundaries in the horizontal direction are again assumed even when they are not explicitly shown. The tensors with red borders are complex conjugates of the ones with the same shape but with black borders. Steps (a-d) are a repetition of what was done in Fig. 25, with some of the intermediate steps omitted. \sim again denotes that the two operators in (d) and (e) have the same spectrum. That they indeed do have the same spectrum is not obvious, but can be shown with an argument exactly like the one used in Fig. 24(e). We have omitted this argument for the sake of brevity. In steps (f) and (h) we use the \mathbb{Z}_2 invariance of u and w to move the spin-flip matrices in the network. In steps (g) and (i) the u and w tensors cancel with their complex conjugates because of their unitarity and isometricity.

individual tensors and does not help in coarse-graining the D_σ defect. Instead we treat the string of D_σ tensors as we would treat any other string of impurity tensors. Coarse-graining such a string can be done using a variation of the usual TNR scheme. The only change is that the unitaries and isometries that are in the vicinity of the D_σ tensors need to be optimized for their respective environments¹⁹. The tensors elsewhere in the network are the same ones used in coarse-graining D_1 . This modified scheme is shown in Fig. 27.

In Fig. 27, we depict the D_σ defect as a two-tensor-wide string. This is because regardless of whether we start with a two-tensor or one-tensor-wide string it is coarse-grained into a two-tensor-wide string at the next scale.³⁶ For the first coarse-graining step we can simply choose $D_{\sigma,I}^{(0)} = D_\sigma$ and $D_{\sigma,II}^{(0)} = A$ and at all later scales the defect will consist of two-tensor-wide string.

The generalized translation operator $T_{D_\sigma}^{(i)}$ is coarse-grained as in Fig. 28. The principle is the same as for $T^{(i)}$ and $T_{D_\epsilon}^{(i)}$, but implementation is not quite as simple because the defect-moving unitary $U_{D_\sigma}^{(i)}$ needs to be contracted with what is essentially a MERA ascending superoperator³⁷ to get the $U_{D_\sigma}^{(i+1)}$ at the next scale. The computational time to perform this coarse-graining of $U_{D_\sigma}^{(i)}$ scales asymptotically as $\mathcal{O}(\chi^{10})$, whereas all the

other steps in the TNR procedure (with or without a defect) are at most $\mathcal{O}(\chi^7)$ ¹⁹, making this step the computational bottleneck.

The argument in Fig. 28 can be generalized to show that a generalized translation by an even number of sites n is coarse-grained to a generalized translation by $\frac{n}{2}$ sites at the next scale, with the unitary $U^{(i+1)}$ being the one defined in Fig. 28(i). Analogously to how a one-tensor string of D_σ 's becomes a two-tensor string under coarse-graining, the two-site operator U_{D_σ} coarse-grains into a three-site operator $U_{D_\sigma}^{(1)}$. Because of this in Fig. 28 $U_{D_\sigma}^{(i)}$ is shown as a three-site operator that is then coarse-grained into a three-site operator $U_{D_\sigma}^{(i+1)}$.

Appendix B: Increasing the period of the conformal spins

The method we present in Sec. III and Appendix A yields conformal spins modulo n , where n is the number of tensors in the transfer matrix. This appendix describes an additional coarse-graining step that can be taken to increase the period to $2n$. We explain how to do this for a model with no defect, but the method can easily be adapted to accommodate for the presence of a defect.

To get conformal spins with a period of $2n$ we want to

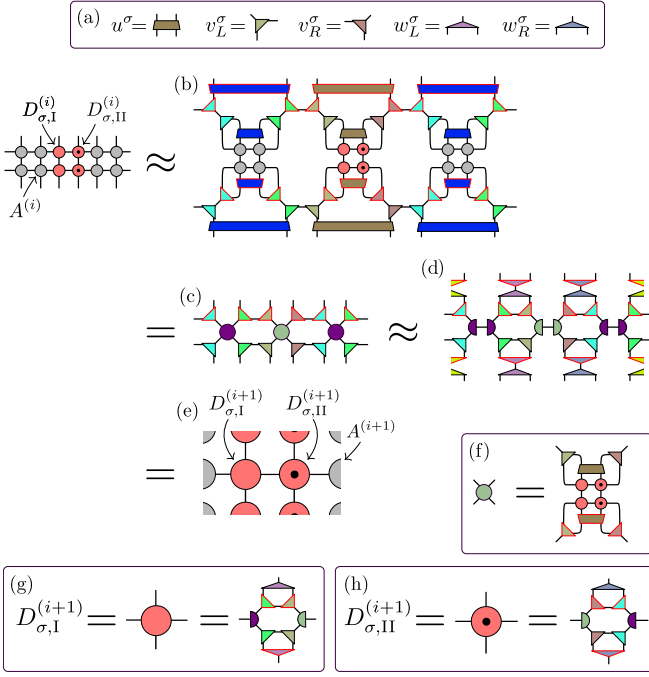


Figure 27. The TNR procedure to coarse-grain a line defect of two tensors. The network is assumed to repeat as similar above and below the part shown, where as on the left and the right it is assumed to consist of tensors $A^{(i)}$. The tensors with red borders are complex conjugates of the ones with the same shape but with black borders. (a) The new tensors used in coarse-graining the defect. They have the same unitarity and isometricity properties as their counterparts in the usual scheme [see Fig. 22]. (b – d, f) The steps of the usual TNR algorithm are repeated for the new isometries and unitaries that coarse-grain the defect. The isometries and unitaries are optimized to again minimize truncation errors, but for the environments that include the $D_{\sigma,I}^{(i)}$ and $D_{\sigma,II}^{(i)}$ tensors. (e) The different tensors are contracted together to form $D_{\sigma,I}^{(i+1)}$ and $D_{\sigma,II}^{(i+1)}$, defined in (g) and (h), that represent the defect at next length scale.

diagonalize the operator $T \cdot M$ of $2n$ tensors. Assume, however, that we can numerically only afford to diagonalize a transfer matrix of n tensors, i.e. a matrix with dimensions $\chi^n \times \chi^n$. We can use an additional layer of isometries to coarse-grain $T \cdot M$ down to n tensors (without changing the bond dimension). The scheme we use to do this is shown in Fig. 29.

This additional coarse-graining does not utilize unitaries the same way TNR does and thus does not remove all short-range correlations. Because of this it causes a truncation error that is relatively large. In practice we find that doing a single such coarse-graining does not qualitatively affect the results: Some accuracy is lost in the scaling dimensions but the conformal spins come out correctly to high accuracy. This lets us match the results obtained with and without the additional coarse-graining and pick the best of both worlds: Use the additional coarse-graining to get the values for the conformal spins

and for the scaling dimensions use values obtained without the additional coarse-graining.

Appendix C: Results for the 3-state Potts model

In this appendix, we present results for the critical 3-state Potts model on the square lattice. It is defined by the partition function

$$Z = \sum_{\{s\}} \prod_{\langle i,j \rangle} e^{\beta \delta_{s_i, s_j}}. \quad (C1)$$

s_i are the local degrees of freedom which take three values, say 0, 1 and 2, and δ_{s_i, s_j} is a Kronecker δ that is 1 only if neighboring degrees of freedom are in the same state and 0 otherwise. The sum and the product are over all configurations and all nearest-neighbor pairs, respectively. The model has a critical point at $\beta = \log(\sqrt{3} + 1)$ and the continuum limit at criticality is described by a $c = \frac{4}{5}$ CFT.

If we permute the three different values of s_i with the same permutation at every site the Boltzmann weights remain unchanged. Thus the 3-state Potts model has a global internal S_3 symmetry, S_3 being the symmetric group for three elements. For every element of S_3 , of which there are 6, there is topological defect for the CFT. We will concentrate here on three elements $\mathbb{1}$, a and a^2 that form the \mathbb{Z}_3 subgroup of S_3 . This is because \mathbb{Z}_3 is Abelian, and manipulating symmetry preserving tensors is computationally much less intensive for Abelian symmetries than for non-Abelian symmetries.

We call the defects related to these three group elements $D_{\mathbb{1}}$, D_a and D_{a^2} and the corresponding twisted partition functions $Z_{D_{\mathbb{1}}}$, Z_{D_a} and $Z_{D_{a^2}}$. As discussed in Sec. VIII, the tensor network methods used for the D_ϵ defect of the Ising model can be generalized to these symmetry defects of the Potts model. Hence we can extract the conformal spins and scaling dimensions of the scaling operators present in the partition functions $Z_{D_{\mathbb{1}}}$, Z_{D_a} and $Z_{D_{a^2}}$.

The numerical results we obtain are shown in Fig. 30. Because of the \mathbb{Z}_3 symmetry each scaling operator comes with a \mathbb{Z}_3 charge, and we have organized the results by this charge. The agreement with the exact values is again excellent. To obtain these results we coarse-grained and diagonalized a transfer matrix of $2^6 \times 4 \times 2^6$ $A^{(0)}$ tensors ($\approx 32\,000$ of the original degrees of freedom). The bond dimensions used in coarse-graining were $\chi = 30$ and $\chi' = 15$. For the conformal spins, a slightly larger system was used, as explained in Appendix B.

Appendix D: Number of degrees of freedom in Z_{D_σ}

In this appendix, we explain the correct way to count the degrees of freedom in a system with a D_σ defect. This affects how we normalize the transfer matrix to extract conformal data.

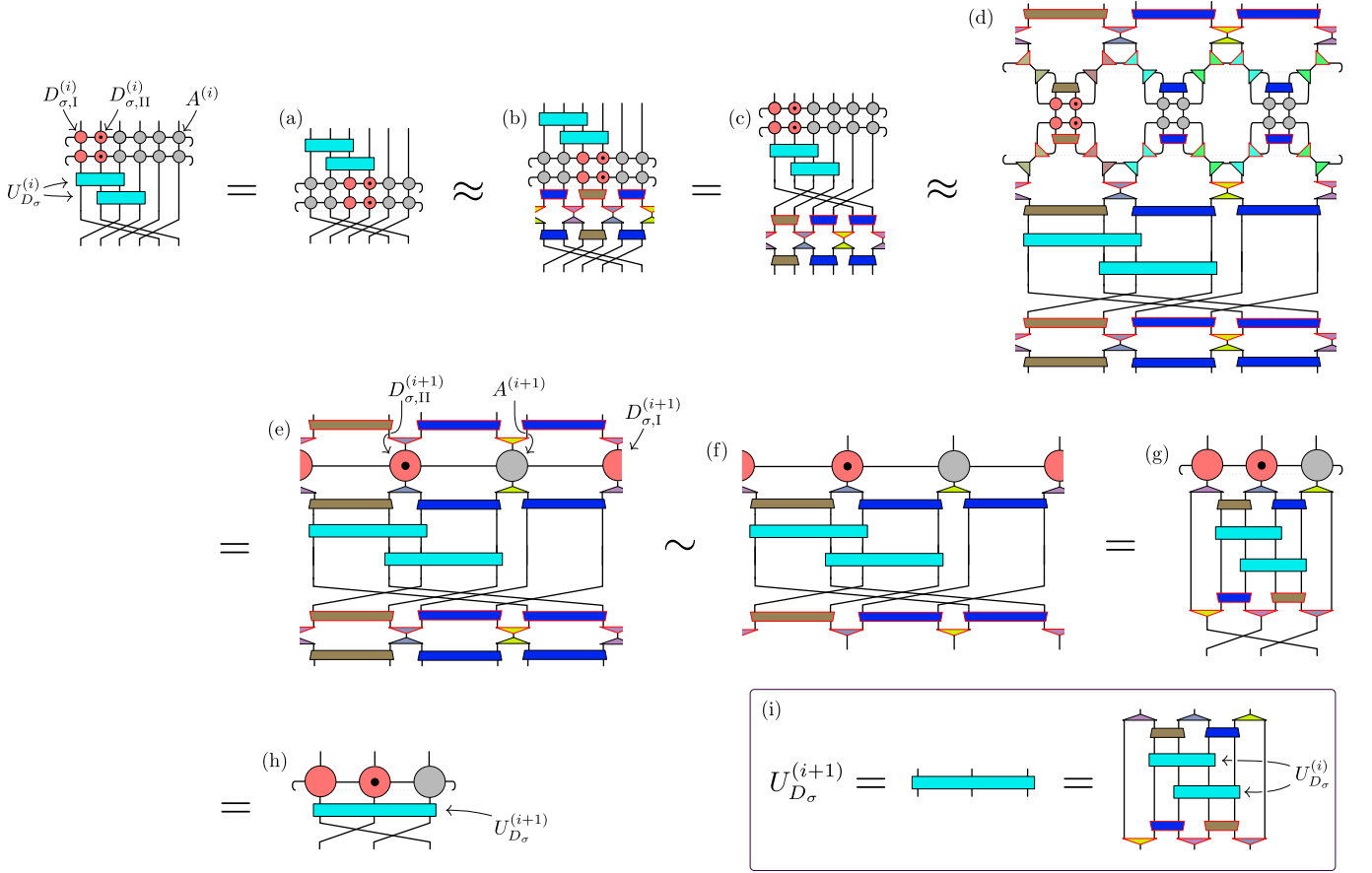


Figure 28. One step of coarse-graining for the operator $T_{D_\sigma}^{(i)} \cdot M_{D_\sigma}^{(i)}$. The generalized translation by two sites gets coarse-grained into a generalized translation by one site at the next scale. Periodic boundaries in the horizontal direction are assumed even when they are not explicitly shown. All the tensors used in these diagrams are familiar from Fig. 27 and Fig. 22 and we have skipped a few intermediate steps that are just a repetition of what is done in those figures. (a) Because $U_{D_\sigma}^{(i)}$ moves the D_σ defect we can move the unitaries to the other side of the transfer matrix as shown. (b) Unitaries and isometries have been inserted into the network. This is like the insertion in the first step of the TNR procedure in Fig. 27, but without the v isometries and only on one side of the transfer matrix. Thus the truncation error introduced by this insertion is at most the truncation error introduced in the TNR step, because less projections are performed. (c) Using again the property that $U_{D_\sigma}^{(i)}$ moves the defect allows us to move the unitaries back to where they were originally. (d) The first step of the TNR procedure in Fig. 27 has been applied to the tensors of the transfer matrix. (e) Some of the tensors have been contracted to form $A^{(i+1)}$, $D_{\sigma,II}^{(i+1)}$ and $D_{\sigma,I}^{(i+1)}$, as in Fig. 25(e). Again, \sim denotes that the operators in (e) and (f) have the same spectrum. This can be shown with an argument exactly analogous to the argument in Fig. 24(e). (g) Pair of unitaries uu^\dagger have canceled and the graph of the network has been reorganized to make it easier to read. (h) The isometries and unitaries have been contracted to form $U_{D_\sigma}^{(i+1)}$, defined in (i). Note that the definition of $U_{D_\sigma}^{(i+1)}$ is nothing but a MERA ascending superoperator acting on two $U_{D_\sigma}^{(i)}$'s.

We build the transfer matrix $M_{D_\sigma}^{(s)}$ from the tensors $A^{(s)}$, $D_{\sigma,I}^{(s)}$, and $D_{\sigma,II}^{(s)}$ and diagonalize it. We use the dependence of $M_{D_\sigma}^{(s)}$ on the system size to determine the free energy term $\ln f$ in the spectrum, as explained in Sec. II, and then normalize this term away. \ln is the number of spins included in the transfer matrix. For the usual Ising model network $Z_{n,m}(A)$ every bond corresponds to a spin and there are twice as many spins as there are $A^{(0)}$ tensors.

However, the bonds on the right side of the D_σ tensor are special: they correspond to only half a spin. This needs to be taken into account when determining f .

That there is half a spin missing can be seen from the way the fusion rules manifest in the lattice models or straight from the explicit form of the D_σ tensor. Perhaps the clearest way is to use the Jordan-Wigner transformation to map the quantum spin chain of n spins into a chain of $2n$ Majorana fermions. There, the D_σ defect is realized as one Majorana mode missing from the chain.

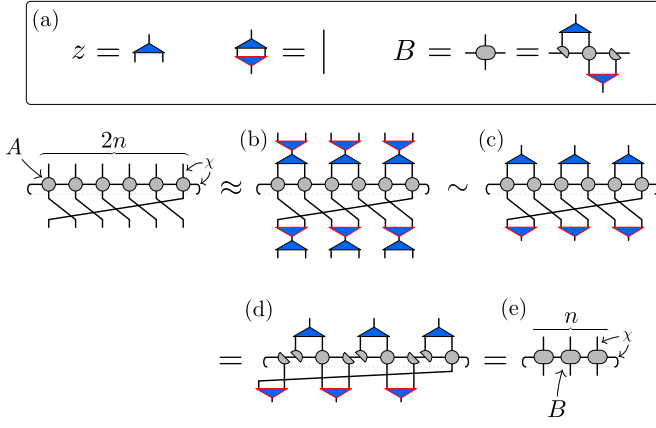


Figure 29. The additional coarse-graining step to increase the period of the conformal spins. The tensors with red borders are complex conjugates of the ones with the same shape but with black borders. (a) z is a coarse-graining isometry, with all of its legs having dimension χ . B is the tensor obtained at the end of the coarse-graining. (b) zz^\dagger pairs have been inserted in the network as approximate partitions of unity. They can be optimized the same way the TNR isometries are optimized, see Ref. 19. (c) \sim denotes that the operators in (b) and (c) have the same spectrum. This can be shown with an argument exactly analogous to the argument in Fig. 24(e). (d) The A tensors have been split into two using a truncated singular value decomposition, as in Levin & Nave's tensor renormalization group²⁰. (e) Some of the tensors have been contracted together into B , defined in (a). The bond dimension of B is the same as the bond dimension of the original tensor A .

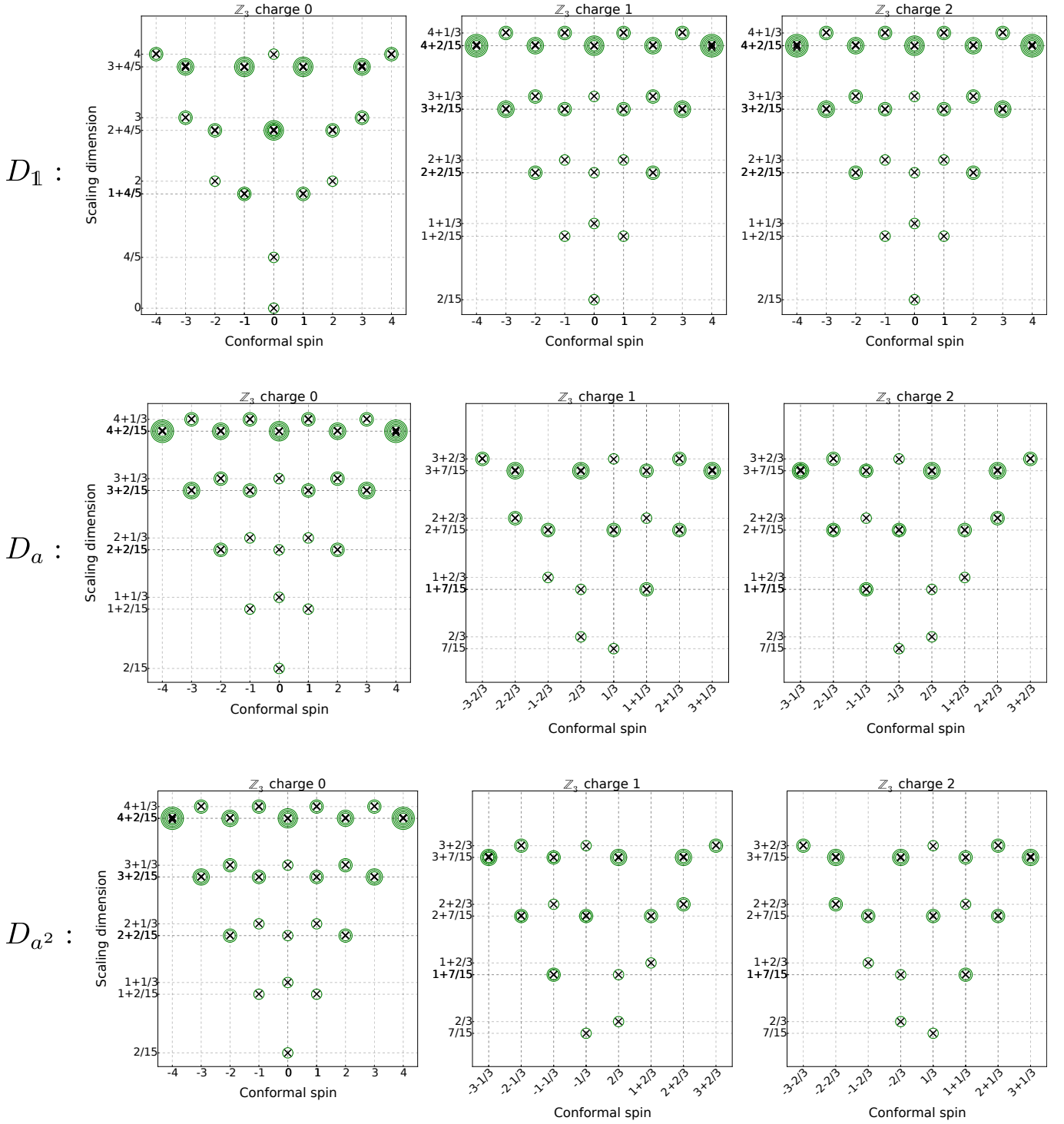


Figure 30. The scaling dimensions and conformal spins of the first scaling operators of the square lattice 3-state Potts model with various defects as obtained with TNR. Every row of three plots includes the results for one of the defects we study: at the top the trivial defect D_1 , in the middle the defect D_a and at the bottom the defect D_{a^2} . Crosses mark the numerical values, circles mark the exact values. Several concentric circles denote the degeneracy N_α of that $(\Delta_\alpha, s_\alpha)$ pair. Although it is not clear from the figure, these degeneracies also come out correctly.